2017

Impacts of ENSO on Tornado Frequency, Intensity, and Geography Across the Eastern United States

Coryn Ann Collins
Louisiana State University and Agricultural and Mechanical College, ccoll82@lsu.edu

IMPACTS OF ENSO ON TORNADO FREQUENCY, INTENSITY, AND GEOGRAPHY ACROSS THE EASTERN UNITED STATES

A Thesis

Submitted to the Graduate Faculty of the
Louisiana State University and
Agricultural and Mechanical College
In partial fulfillment of the
Requirements for the degree of
Master of Science

in

Geography and Anthropology

by
Coryn Ann Collins
B.S., Texas A&M University, College Station, 2015, Meteorology
May 2017

ACKNOWLEDGEMENTS

First and foremost, I would like to thank my advisor, Dr. Barry Keim. There is no way I could ever fully express the gratitude I have for your endless guidance, fatherly wisdom, and of course, many happy hours. I would also like to thank my other committee members, Dr. Alan Black, Dr. Ashton Robinson-Cook, and Dr. Lei Wang, for taking so much time out of their busy lives to help me accomplish this research. I'm also grateful for the other professors in the department, who gave me tools in the classroom to perform a lot of this research. I must also thank NOAA's RISA team for funding this research, without which I would not be here to begin with.

A huge shout out to all my grad school gal (and guy) pals for giving me a home away from home. I owe not having too many mental breakdowns to you guys. Tess – the best roommate a girl could ever want – thank you for having my back for all the ups and downs, for not tossing my cats out on the street, and giving me one more lifelong friend.

Finally, I have my entire family to thank. I have my grandfathers, Dandy and Traddy, to thank for encouraging me to pursue science and weather. Thank you to my sister, Cayla, for giving me the stability I never knew I needed until you moved here. Mom – you've been my biggest supporter since day one, and you push me to believe in myself every single day. I would not be the successful woman I am today without having a role model like you. But of course, I wouldn't have finished without the love and support of my best friend and partner in life, Josh. Thank you for not only dealing with two years of LDR, but constantly reminding me that I could do this. Now I finally have proof that I'm smarter than you!! But really, I love you.

TABLE OF CONTENTS

ABSTRACT

Tornadoes are a reoccurring severe weather hazard, with the highest rates globally occurring in the central United States. Despite their high frequency in the U.S., the scientific community's disagreement of tornado activity during varying phases and intensities of the El Niño Southern Oscillation (ENSO) justifies a need for further research. In this study, tornado events from 1950 to 2014 in the U.S. east of the Rocky Mountains were investigated for seven phases of ENSO: strong, moderate, and weak El Niño/La Niña and the neutral phase. A seasonal Niño 3.4 index was used as the definition of ENSO. ENSO influences on tornado frequency, intensity, geographical distribution, and track area were tested using sophisticated mapping (i.e. GIS optimized hot spot analysis) and spatial statistics (i.e. average nearest neighbor and global Moran's I). Results indicate that in spring, a Weak La Niña correlates with higher tornado intensity and stronger, long-lived tornadoes that shift eastward from the central U.S. as ENSO transitions from El Niño to La Niña. Summer has high tornado frequencies that do not vary dramatically across ENSO phases, with weak, short-lived tornadoes occurring in tornado outbreaks. Fall has similar tornado frequencies across six of the seven ENSO phases, apart from largely higher annual counts during a Strong La Niña phase. Winter exhibits more tornadoes that are stronger and longer-lived during a Moderate La Niña phase, with a northward expansion in tornado hot spots as ENSO transitions from El Niño to La Niña. In general, La Niña is most conducive for higher tornado counts and stronger, longer lived tornadoes.

CHAPTER 1: INTRODUCTION

1.1 Background

Severe thunderstorms are capable of producing violent tornadoes across the eastern United States. Second to hurricanes, thunderstorms producing tornadoes, along with hail and powerful winds cost the U.S. an average of about $1.6 billion in damage per year (Munich 2013). While many studies have been implemented to better understand tornadic dynamics, the scientific community has not fully developed a single theory that explains all the observed features in a tornado (Rotunno 1986). Furthermore, our understanding of the influence and impacts of atmospheric teleconnections, such as the El Niño Southern Oscillation (ENSO), on the tornado climatology in the U.S., while having improved in recent years (Cook and Schaefer 2008, Allen et al. 2015) has plenty of room for improvement.

There are disagreements in the scientific community about the effects of teleconnections, such as ENSO, on tornado climatology. First, this type of study is complicated due to a scaling problem. Tornadoes are considered "mesoscale", or very localized, making it difficult to adequately capture the effects of large-scale and long-term atmospheric processes (Trenberth and Stepaniak 2001). Another complication with the tornado record is that the number of tornado reports has increased dramatically through time. This is due to improvements in tornado detection technology (i.e., Doppler radar), increased eyewitness reports from population increases over time, and changes in damage survey procedures (Lee et al. 2013). Other problems, such as underreporting of tornadoes and the likely underrating of tornadoes due to lack of structures for damage reports are also contributors to the complexity of these studies (Brooks and Doswell 2001).

Researchers have used varying techniques to better understand how ENSO effects

tornadic frequency and density in the Continental United States (CONUS). However, many of these studies have contradicting results due to varying methods. Bove (1998) saw a reduction [increase] of tornadic activity in the southern plains during El Niño [La Niña]; El Niño [La Niña] inhibits [facilitates] large tornado outbreaks. A northward displacement of the subtropical jet stream during La Niña brings stronger dynamical forcing (i.e. forced lifting of air) to parts of the southeast U.S. (Ropelewski and Halpert 1989), creating an environment more conducive for tornadoes. On the contrary, El Niño shifts the subtropical jet stream southward, removing this forcing from the U.S. which makes the environment less conducive for tornadoes. Tornadoes commonly develop in spring due to the large difference between cold, dry air masses pushing southward from Canada and warm, moist air moving northward from the Gulf of Mexico (GOM) (Bove 1998). This large difference, also referred to as the temperature gradient, creates atmospheric instability conducive for severe weather. El Niño [La Niña] events tend to decrease [increase] the temperature gradient between these two air masses, and is therefore less [more] conducive for tornadic activity. These results were consistent with other similar studies (Monfredo 1999; Marzban and Schaefer 2001; Lee et al 2013; Allen et al. 2015; Lee et al. 2016).

However, not all of the literature agrees with these findings. Agee and Zurn-Birkhimer (1999) suggest that the phase of ENSO does not have a role in the production of stronger or longer track tornadoes, regardless of phase. Knowles and Pielke (2005) claim that there is little difference found in total numbers between El Niño and La Niña events. They do confirm that La Niña events do tend to have longer tracked, more violent tornadoes than El Niño. Warmer than normal temperatures in the northwest pushing against colder than normal temperatures in the south during El Niño years weakens the interactions between the two air masses, decreasing the lengths of tornadoes, and the opposite is true for La Niña years (Knowles and Pielke 2005). Cook

and Schaefer (2008) found that ENSO neutral years actually have the strongest correlation with an increase in tornado days (a day with 6 or more tornadoes), with respect to El Niño and La Niña. Finally, Schaefer and Tatom (1999) agree with Knowles and Pielke that the phase of ENSO does not favor tornado frequencies, and solely exhibit a shift in geographic location in the Mideastern and Northeastern United States during a La Niña phase. Their hypothesized physical explanation for this is little or no lag between warm/cold Pacific water and associated weather (Schaefer and Tatom 1998). This discordance amongst aforementioned studies is an issue that needs to be resolved.

1.2 Statement of Problem

A key goal of this study was to ease the aforementioned conflict in the literature. To do this, seven different categories of ENSO were examined to see their effects on spatial and temporal tornadic variability and characteristics. While other studies have looked at three phases of ENSO (El Niño, La Niña, and Neutral), this study will represent an improvement of the current science by looking at the following seven categories:

1. Strong El Niño
2. Moderate El Niño
3. Weak El Niño
4. Neutral
5. Weak La Niña
6. Moderate La Niña
7. Strong La Niña

This study will also contribute to the literature by looking at ENSO influences in all seasons. Cook and Schaefer (2008) analyzed tornado activity in winter, and Lee et al. (2013) and Lee et al. (20016) both analyzed tornado activity in spring, but only one other study has looked at the influence of ENSO on tornado activity year-round (Allen et al. 2015). It is hypothesized

that the reason for varying results amongst previous studies is because the intensity of ENSO has not been taken into account, which could have led to contradictory results. The overlying purpose of this study is to examine how these varying ENSO categories affect seasonal tornadic characteristics and tendencies.

1.3 Objectives

This thesis represents an improvement in the literature by not only examining seven phases of ENSO, but also by analyzing relationships during four seasons: Winter (DJF), Spring, (MAM), Summer (JJA), and Fall (SON). Therefore, the major objectives of this paper are to build on previous studies by examining the effects that ENSO has on tornadic characteristics and tendencies seasonally from 1950-2014. The statistical significance of all findings, for both spatial and temporal trends, was also analyzed. As such, objectives of this research are to:

1. To analyze tornado frequencies for the entire tornado record, and for weak (EF-0 and EF-1) and strong (EF-2 through EF-5) tornadoes as they relate to intensities of ENSO
2. To analyze the geographical distribution of tornadoes by ENSO phase.
3. Analyze tornado days and the Destruction Potential Index as a function of ENSO to better understand tornado outbreaks and track area
4. Produce results which ease conflict in the literature.

These objectives will be met through the seven class ENSO system, sophisticated mapping, spatial statistics, and atmospheric composite analysis. The following two chapters will accomplish these objectives, and are written in journal-style formatting which may help shed some light on the problem with these types of studies. The next chapter will primarily focus on spatial distribution and tornado frequencies as a function of ENSO phase and intensity. The following chapter will cover this same relationship, shifting focus towards weak and strong

tornadoes, as well as tornado days and the Destruction Potential Index. The thesis will then have a concluding chapter that summarizes the findings for each of the objectives noted above.

CHAPTER 2: SPATIAL ANALYSIS OF TORNADO FREQUENCY AS A FUNCTION OF ENSO IN THE EASTERN UNITED STATES

2.1 Introduction

Tornadoes pose a significant threat to lives and property across the United States, and can result in large losses of both (Farney et al. 2015). Although the tornado record has become more robust due to improvements in tornado detection technology (i.e., Doppler radar), increased eyewitness reports from population increases over time, and changes in the damage survey procedures (Lee et al. 2013), our vulnerability to these events is still considerable. The record-breaking tornado outbreak of April 2011 is just one example of their destruction. During this event, there were 1084 tornadoes, 5,182 injuries, 541 deaths, and over $9 trillion in estimated property loss (Lee et al. 2013; SPC 2016). It just so happens that the spring of 2011, when that tornado outbreak occurred, the tropical Pacific was transitioning from a Moderate La Niña to a Weak La Niña, thereby raising suspicion that the event may be linked to this teleconnection (Lee et al. 2013). Previous studies have also shown a linkage of tornado activity in the Eastern United States to La Niña phases (Monfredo 1999; Marzban and Schaefer 2001; Lee et al 2013; Allen et al. 2015; Lee et al. 2016), but knowing the role that the intensity of the El Niño-Southern Oscillation (ENSO) plays would be beneficial to seasonal tornado outlooks.

This chapters aims to discover the temporal and spatial characteristics of tornado activity as a function of ENSO intensity. While previous studies have analyzed seasonal tornado frequency and geographic distribution as a function of ENSO (Schaefer and Edwards 1999; Marzban and Schaefer 2001; Cook and Schaefer 2008), no studies have analyzed the relationship as a function of ENSO intensity as well. Understanding the geographical variability of tornadoes

during each phase of ENSO could potentially result in improved seasonal forecasts for such activity in the United States. This chapter examines the temporal change in tornado frequency and distribution from 1950 through 2014. The statistical significance of both spatial and temporal trends was analyzed for confidence. As such, the objectives of this research are to:

1. To analyze tornado frequencies across the eastern United States as they relate to intensities of ENSO
2. To analyze the seasonality of tornadoes across the eastern United States
3. To analyze the geographical distribution of tornadoes as related to ENSO
4. Produce results which ease conflict in the literature

2.2 Data

Studies examining ENSO and tornados have utilized various definitions of ENSO, such as the Trans-Niño Index (Lee et al. 2013), the Climate Prediction Center's definition (Marzban and Schaefer 2001; Cook and Schaefer 2008), the Japan Meteorological Agency Index (Bove 1998), and the Oceanic Niño Index (Cook and Schaefer 2008). Cook and Schaefer (2008) also used a "4-tier" classification system to identify tornado outbreaks, and found that the definition of ENSO did not change the results by much. The Oceanic Niño Index (ONI), used in a more recent study (Allen et al. 2015), was stratified into a useful list of ENSO intensities by Golden Gate Weather Services (Null 2016). ONI values are a running 3-month mean of sea surface temperature (SST) anomalies in the Niño 3.4 region, and are positive for El Niño, and negative for La Niña. For example, a moderate La Niña would fall between -1.0 and -1.4. The intensities of ENSO are categorized under the following magnitudes:

- Weak: 0.5 - 0.9
- Moderate: 1.0 - 1.4

- Strong: Equal to or larger than 1.5

However, because the ONI is calculated using a running 3-month mean, it would not be useful for a seasonal analysis as a function of ENSO since it would include values in the months surrounding the season. Therefore, a seasonal Niño 3.4 index was used. Seasons were categorized as: Winter (DJF), Spring (MAM), Summer (JJA), and Fall (SON). Data were retrieved from the Climate Prediction Center's Monthly Atmospheric and SST Indices database (CPC 2016). The monthly Extended Reconstructed SST (ERSSTv4) anomaly dataset with centered base periods was used because of its monthly input into the ONI (CPC 2016), as well as its detrended mean for producing SST anomalies. A centered SST dataset was chosen as opposed to a one with a 1981-2010 base period because this analysis began in 1950. Centered base periods detrend SST anomalies so that external variables such as climate change or an increase in SSTs are not an influence. With a 1981-2010 base period for an analysis starting in 1950, the adjusted average for a year early in the record (i.e. 1950) would be much warmer than what was observed from the increase in SSTs, indicating a higher mean for that year and resulting in a higher anomaly. Since the Niño 3.4 index values are an average SST anomaly value similar to the ONI, the same intensity thresholds from the ONI were used. It should be noted that averaging monthly SST values over a season pulls the distribution away from the extremes and towards weaker ENSO and neutral phases. Each season was binned into a Strong El Niño (SEN), Moderate El Niño (MEN), Weak El Niño (WEN), Neutral, Weak La Niña (WLN), Moderate La Niña (MLN), or Strong La Niña (SLN) category based on its 3-month average SST anomaly value. A complete list of seasonally binned years for each ENSO phase are in the Appendix.

The Storm Prediction Center's Tornado Database provided the critical tornado information necessary for this analysis; primarily, tornado touchdown points (Schaefer et al.

1980; Schaefer and Edwards 1999). These points, which are originally imported in a WGS84 coordinate system, were projected into a Lambert Conformal Conic projection. This projection is utilized because it is one of the best for mid-latitudes (ESRI 2016), where the study area is located. A conic projection starts at a single point over the poles, then extends southward in a cone shape. This projection works best for all areas that have a greater east-west extent, like the United States (ESRI 2016). The Lambert Conformal was chosen over another conic projection, such as the Albers, because it portrays shape more accurately than area, which is a feature desired for this study. Both an 80km grid and a 40km grid are used by the Storm Prediction Center, but a 40km grid is used as the grid of choice when analyzing count data due to its extensive use by the SPC (SPC 2016; Figure 2.1). The number of tornado touchdowns in each 40km grid cell were tabulated and used as the primary data source in this analysis.

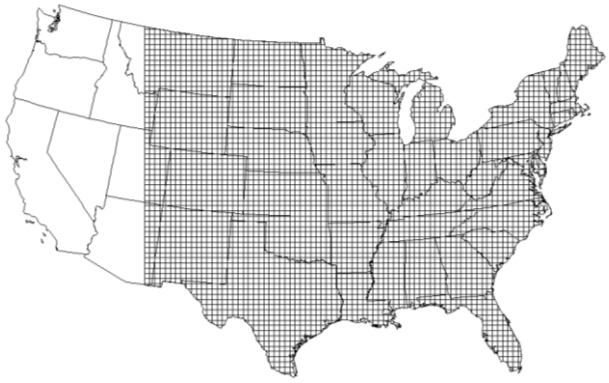

Figure 2.1. A 40-km grid depicting the study region chosen for this study.

Lastly, atmospheric composites were plotted for a better understanding of upper and lower air conditions during varying phases and intensities of ENSO, and their relationship with tornadic counts and spatial distribution. Atmospheric variables including 500hPa geopotential height contours, 500hPa geopotential height anomalies, 850hPa wind vectors, and 300hPa wind vectors were plotted using data from ESRL's Monthly and Seasonal Climate Composites (ESRL

2016) for each season and phase/intensity of ENSO.

2.3 Methods and Results

2.3.1 Spatial Statistics Indicators

To determine whether there is evidence of clustering in tornado incidents, two global indices of spatial autocorrelation were calculated: average nearest neighbor and global Moran's I. Average Nearest Neighbor calculates a nearest neighbor index based on the average distance from each feature to its nearest neighboring feature (ESRI 2016). A random pattern generated from the Poisson process is compared against the real data to measure the strength of clustering. The null hypothesis is that the two processes are similar, or that there is no clustering and the features are randomly distributed. This tool was implemented on each season per ENSO category, resulting in a total of 24 statistical outputs based on available data. The second tool, Global Moran's I, was used to verify and analyze spatial clustering through a different method. Given a set of features (i.e. tornado touchdown points) and an associated attribute (count data), this tool evaluates whether the pattern expressed is clustered, dispersed, or random (ESRI 2016). The associated attribute (count data) is derived from the number of points assigned to each cell in the 40km grid, resulting in a "count" number per fishnet grid. Again, the null hypothesis states that the values associated with the features are randomly distributed. For both analyses, z-scores were used to compare across phases and intensities of ENSO to determine which category has the strongest spatial clustering. Results also indicate if z-scores are similar or different, thereby determining which phases/intensities of ENSO have the largest effect on spatial autocorrelation amongst tornado counts. Figure 2.2 shows the z-scores for both analyses across each phase of ENSO by season.

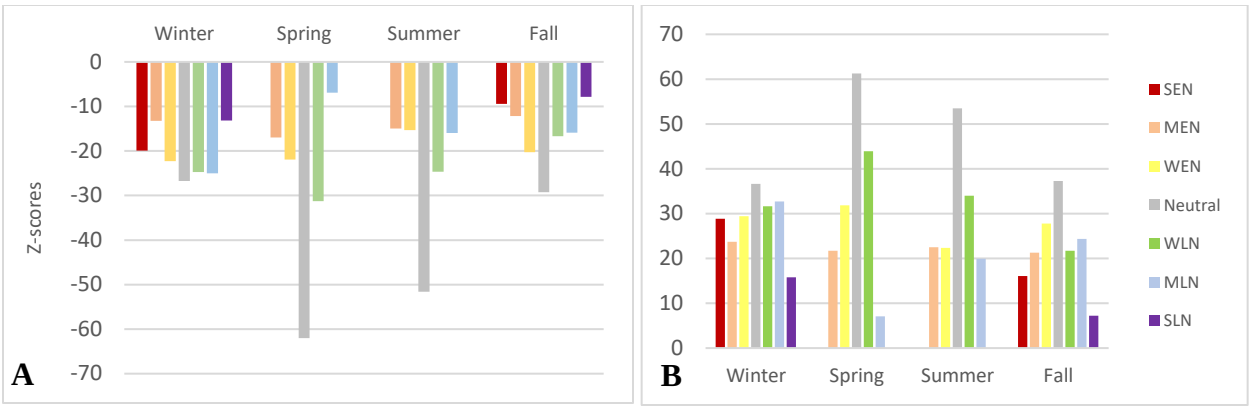

Figure 2.2: Average nearest neighbor (A) and Global Moran's I (B) z-scores across phases and intensities of ENSO

All groups came back with significant p-values, rejecting the null hypothesis that the features are randomly distributed (i.e. no clustering). This was for all tornadoes in the record. The strength of clustering is represented by z-scores; a larger absolute value indicates stronger clustering. It should be noted that spring and summer SEN and SLN had zero tornado counts and are excluded from this series of analyses. For each category, the Neutral phase has the strongest clustering amongst all seven phases. Considering this is the category with the most tornadoes across all four seasons, this is not surprising. If we remove the influence of the ENSO neutral phase, in two out of four phases WLN has the strongest clustering (spring and summer). Apart from spring and summer, where there are zero representatives in the stronger categories, SLN had the weakest spatial clustering. SEN also has weak spatial clustering in fall, but is relatively large in winter. In spring, summer, and fall, the degree of spatial clustering generally weakens as the phase of ENSO becomes stronger. This could be due to the dampening of sample sizes as ENSO strength increases. Winter does not follow this same pattern, where all z-scores are similar apart from MEN and SLN. Comparing across seasons, SEN has the strongest clustering in winter and the weakest in fall. MEN has relatively consistent Z-scores across all seasons, but WLN has the strongest clustering in spring which decreases in the other seasons. Out of the seven categories,

winter has the strongest spatial clustering for four phases of ENSO – SLN, MLN, MEN, and SEN. The fall season has the weakest clustering in four ENSO categories.

2.3.2 Seasonal Hot Spots

Seasonal hot spot maps were created in GIS through the "Optimized Hot Spot Analysis" tool. Given incident points (i.e. tornado touchdown locations), this tool creates a map of statistically significant hot and cold spots using the Getis-Ord Gi* statistic (Getis and Ord 1992; ESRI 2016). Getis-Ord Gi* works by examining each feature within the context of neighboring features, or nearby tornado origin points. The local sum for a feature and its neighbors is compared proportionally to the sum of all features, and when the local sum is much different than the expected local sum and the difference is too large to have resulted from random change, it is scored a statistically significant z-score (Mitchell 2005). For statistically significant (p-value less than or equal to 0.05) and positive z-scores, larger z-scores indicate more intense clustering of high values (hot spots). For statistically significant and negative z-scores, smaller z-scores indicate more intense clustering of lower values, or cold spots (ESRI 2016). Equations used in this statistic are accessible on ESRI's "Optimized Hot Spot Analysis" page (ESRI 2016).

GIS offers two types of hot spot tools – the standard Hot Spot Analysis (Getis-Ord Gi*), as well as the Optimized Hot Spot Analysis tool. For the purpose of this study, the latter method was utilized for several reasons. The Optimized Hot Spot tool automatically aggregates incident data, identifies appropriate scale of analysis, and corrects for both multiple testing and spatial dependence (ESRI 2016). The automatic aggregation of data allowed the input data features to be the original Conformal Lambert Conic projected tornado touchdown points. This tool also determines settings to produce optimal hot spot analysis results. Most importantly, it identifies statistically significant spatial clusters of hot and cold spots, which are useful in this study to

identify local tornado clusters as a function of ENSO intensity and phase. Figure 2.3 shows plots representing ENSO hot spots for all four seasons, resulting in a total of 28 individual figures (four of which have no tornadoes, and are labeled appropriately). Each hot spot analysis is defined by a seven-category legend: hot and cold spots with 90%, 95%, and 99% confidence, as well as non-significant spots.

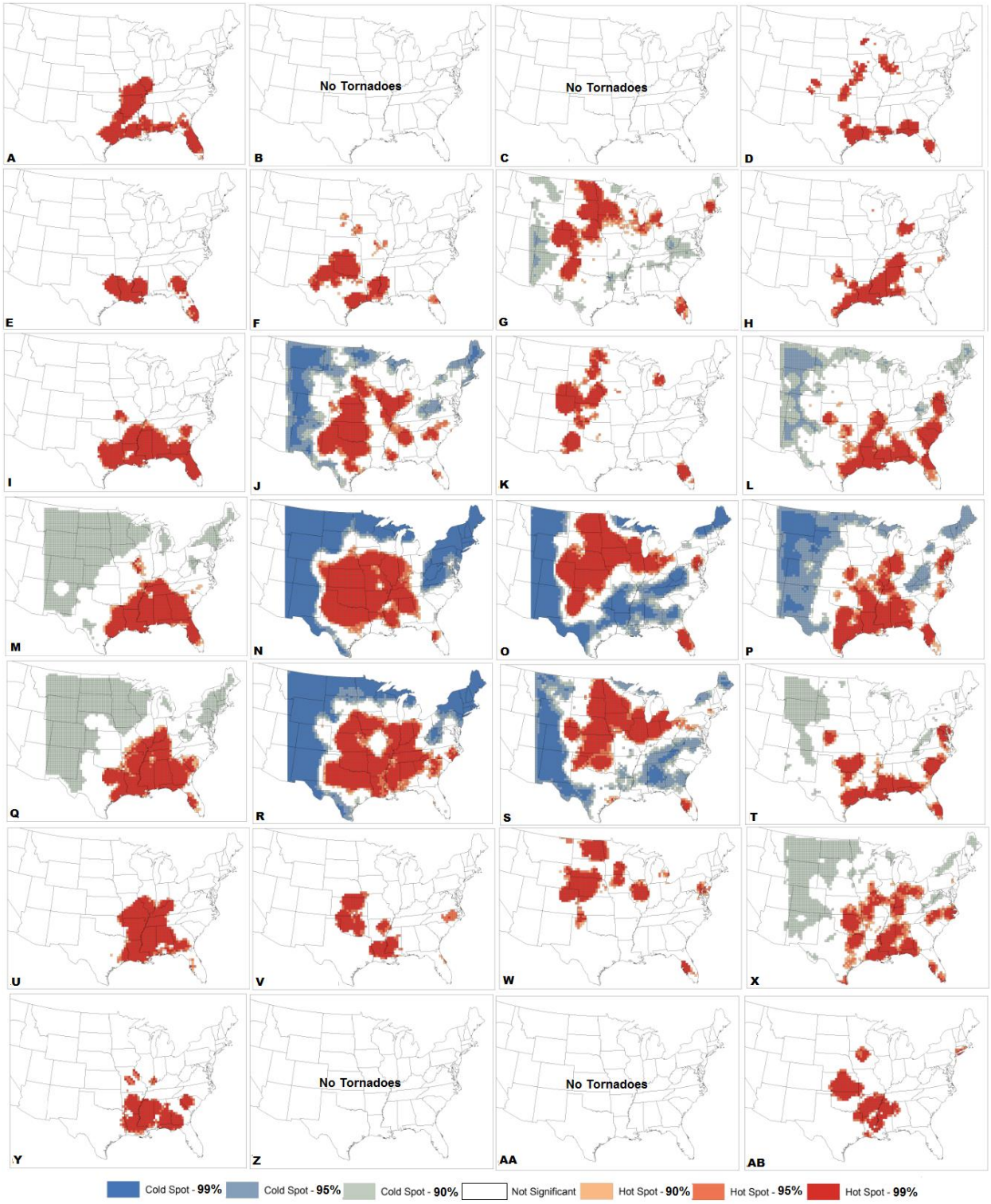

Figure 2.3: Tornado hot and cold spots, 1950-2014. Columns are in the order of winter, spring, summer and fall. A-D are Strong El Niño, E through H are Moderate El Niño, I through L are Weak El Niño, M through P are Neutral, Q through T are Weak La Niña, U through X are Moderate La Niña, and Y through AB are Strong La Niña.

Changes in spatial distribution of severe thunderstorm activity are attributed to the position of the jet stream (Barnes and Newton 1986; Johns and Doswell 1992; Cook and Schaefer 2008). The jet stream is modified by phase and intensity of ENSO (Cook and Schaefer 2008, Allen et al. 2015), as well as changes in season (Fraunfeld and Davis 2003; NWS 2016). Understanding the location of the jet stream is important because synoptic scale disturbances tend to form in areas of maximum wind speed and follow jet axes (Holton 1992), which modulates the location and intensity of severe weather (Archer and Caldeira 2008) and potentially tornado activity. The circumpolar vortex, which is a complex upper-level low-pressure area over the North Pole, is defined by geopotential contours that lie within the core of tropospheric westerlies (Frauenfeld and Davis 2003). Expansion (contraction) of the circumpolar vortex results in equatorward (poleward) modulation of the jet stream. Seasonal analysis revealed that the largest shift in the jet stream and geopotential heights in the Northern Hemisphere was during summer in the circumpolar vortex (Frauenfeld and Davis 2003). The average latitude of the jet stream begins to shift poleward during spring, shifts most evidently northward during summer with the contraction of the circumpolar vortex, then retreats towards the Equator in fall (NWS 2016). However, the intensity of the jet stream is strongest during winter, since the jet stream follows gradients between warm and cold air, which is most pronounced during winter (NWS 2016). Spatial evolution of hot spots in Figure 2.3 generally reflect the seasonal evolution of the circumpolar vortex and attendant jet stream.

In winter, hot spots consistently lie along the GOM regardless of ENSO phase. In all three phases of ENSO (Figure 2.3A, 2.3E, 2.3I), there are hot spots along Florida, which is consistent with extratropical cyclogenesis in the GOM during El Niño years (Hardy and Hsu 1997). As ENSO transitions from El Niño to La Niña phases, tornado hot spots shift further

northward (Figure 2.3Q, 2.3U) with the exception of the SLN phase (Figure 2.3V). This is likely due to the northward displacement of the jet stream during La Niña phases (Cook and Schaefer 2008). A stronger La Niña tends to exhibit more northerly tornado activity; the exception during a SLN phase is likely due to a decrease in sample size.

Spring has persistent hot spots along the central U.S. regardless of ENSO phase and intensity. This is consistent with Brooks et al. (2003), where tornado activity during spring is more active along the central plains. However, as ENSO transitions from El Niño (Figure 2.3F, 2.3J) to La Niña (Figure 2.3R), the location of these hot spots generally shifts eastward through a WLN phase. The sudden decrease in hot spots during a MLN is likely due to a dampening in sample size, and will be discussed in section 2.3.3. There is also an increase in tornado activity further north during Neutral (Figure 2.3N) and WLN (Figure 2.3R) phase, which is likely due to the northward displacement of the jet stream during a La Niña phase, moving the storm track northward as well.

Regardless of ENSO phase and intensity, tornado activity in the summer primarily lies along the north-central U.S. corridor. Frauenfeld and Davis (2003) found that the circumpolar vortex is strongest during the summer, which contracts the jet stream northward and subsequently the storm track also shifts northward. When comparing across ENSO phases (Figure 2.3, column 3), it is seen that the location of these hot spots really doesn't change dependent upon the phase of ENSO. Decreases in tornado hot spot area is likely due to smaller sample sizes during ENSO extremes (moderate phases) compared to weak phases and a neutral state. ENSO does not seem to play a role geographically in tornado activity during summer.

Finally, in fall, there is not a discernable shift in tornado hot spots dependent on ENSO phase (Figure 2.3, column 4). All phases exhibit tornado activity primarily along the GOM,

which is caused by a southwardly displaced jet stream. However, it does seem that tornado hot spots are more aggregated during El Niño phases (Figure 2.3D, 2.3H, 2.3L) than La Niña phases (Figure 2.3T, 2.3X, 2.3AB). This is verified by global spatial statistics (Figure 2.2A and 2.2B), which indicate stronger clustering during El Niño phases and weaker clustering during La Niña phases when comparing ENSO intensities against each other (i.e. SEN vs. SLN).

2.3.3 Adjusted Tornado Counts

To eliminate the upward trend in tornado counts over time due to factors such as urbanization, population increase, and improvement in radar technology (Brooks et al. 2003; Lee et al. 2016), the Storm Prediction Center developed a simple method to eliminate this issue using a linear regression equation (Brooks and Carbin 2007). An analysis on raw tornado counts during varying phases of ENSO might be questioned due to the obvious upward trend in reports since 1950, necessitating this detrended analysis. While this method can remove the trend in tornado reports due to changes in detection and reporting, it cannot remove the potential influence of other external variables such as climate change and additional teleconnections. Figure 2.4 is an example of one of these calculations, which compares the raw values (Figure 2.4A) and adjusted values (Figure 2.4B).

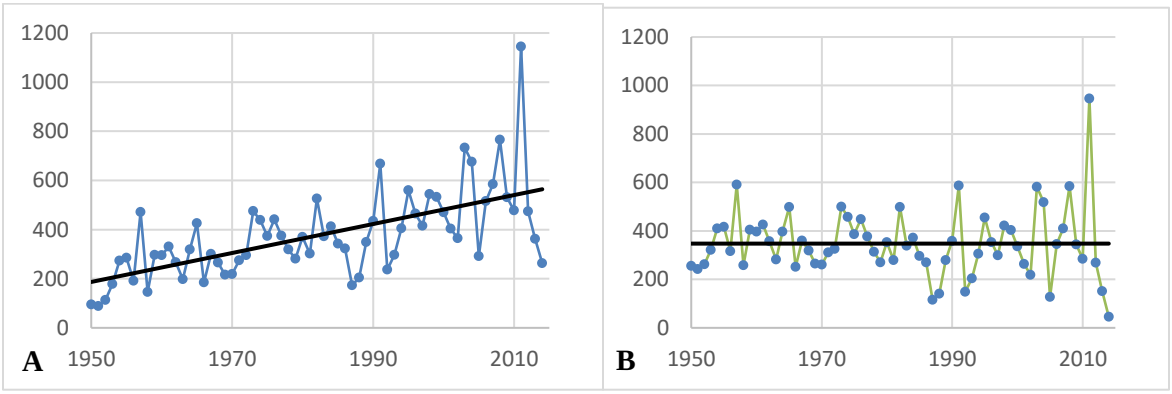

Figure 2.4: Raw (A) and adjusted (B) tornado counts in spring, 1950-2014

Annual tornado frequency is first plotted from 1950-2014. This upward tick in tornado counts is easily visible with a linear trend line, shown in black. The linear trend line equation is used to compute the "delta", which is the linear equation value for that year minus the original annual total, which results in the adjusted tornado count for that year (Brooks and Carbin 2007). For raw tornado counts in the spring (Figure 2.4A), the median was 348. Each individual delta (positive if the original value is above the trend line, negative if below) was applied to 348. The resulting value is the adjusted tornado count for that year. Detrended tornado counts were calculated for all four seasons. Detrending the tornado counts helped to analyze tornado counts during different phases and intensities of ENSO. Once an adjusted tornado count has been calculated for each year and each season, counts can be binned into their appropriate ENSO category per year. The total sum of each ENSO category was calculated, then averaged to eliminate the influence of heavily represented categories in respect to lesser-represented categories (i.e. neutral categories versus stronger categories). The results are in Figure 2.5. The average values were then used for statistical tests examining the difference of means, such as the Kruskal-Wallis and Mann-Whitney test.

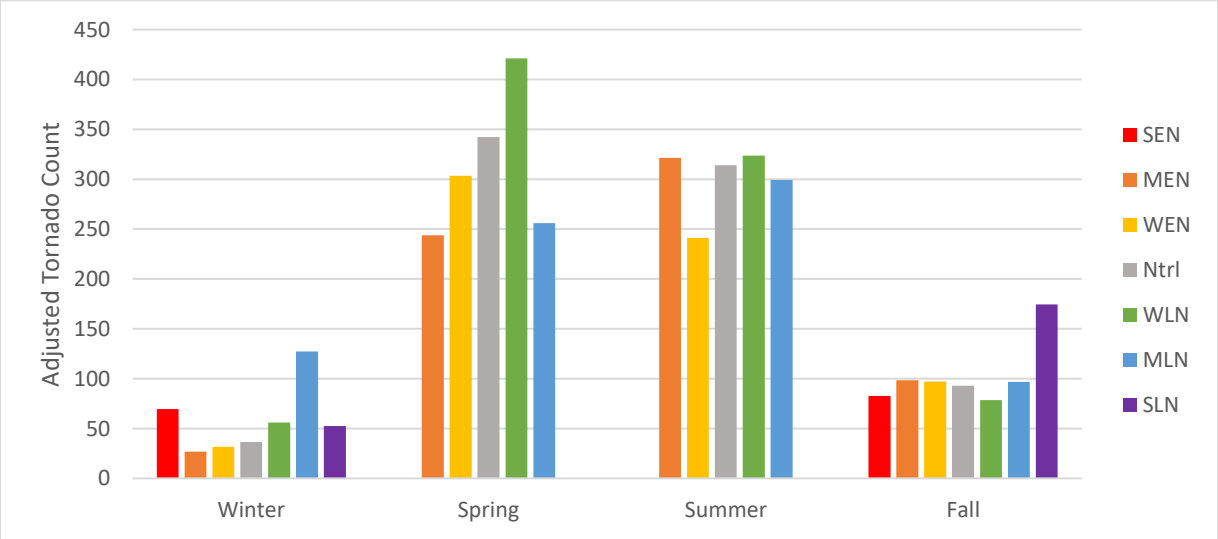

Figure 2.5: Detrended tornado counts per season across all phases of ENSO, 1950-2014

To determine which statistics test was most applicable to the adjusted tornado counts, the data were tested for normality using both the Shapiro-Wilk test and Normal Quantile-Quantile (Q-Q) plots in R. When checking for normality, Q-Q plots are used to compare a sample distribution (i.e. adjusted tornado counts) with a theoretical sample (i.e. a normal distribution, with a mean of zero and a standard deviation of one) (Vries and Meys 2015). The Shapiro-Wilk test was also used to either confirm or deny the findings from the Q-Q plots. The null hypothesis for the Shapiro-Wilk test is that the sample comes from a population which has a normal distribution (Royston 1982). Significant p-values would reject the null hypothesis, indicating that the sample has non-normal properties. The results for all four seasons, with their respective Shapiro-Wilk p-values, are shown in Figure 2.6.

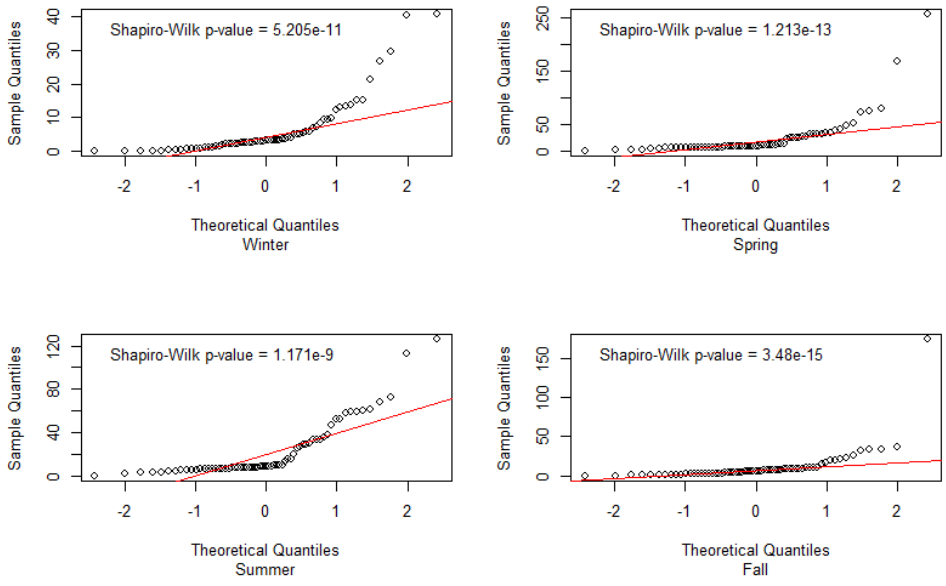

Figure 2.6: Seasonal normal Q-Q plots with Shapiro-Wilk p-value.

With statistically significant p-values of less than .01 rejecting the null hypothesis of normality, as well as different observed and theoretical (in red) distributions from the Q-Q plots, it is determined that the distribution of all four datasets should be tested using non-parametric statistics. To test the differences between ENSO phases on a non-normally distributed

continuous variable (i.e. count), the Kruskal-Wallis test is most appropriate because these data are unpaired (Kruskal & Wallis 1952; McKight and Najab 2010). The null hypothesis of the Kruskal-Wallis test is that there are not any statistical differences between two or more groups of an independent variable (Aerd 2016). The results of the Kruskal-Wallis test are in Table 2.1.

Table 2.1: Kruskal-Wallis rank sum resulting p-values

Season	P-value
Winter	< 0.001
Spring	< 0.001
Summer	< 0.001
Fall	< 0.001

Significant p-values reject the null hypothesis that there are no differences between two or more groups – in this case, "groups" are different phases of ENSO during each season. Therefore, these p-values indicate that at least one ENSO phase is different from the others. To test and specify exactly which ENSO phases are different from each other, the Mann-Whitney test was used. This test was used over the Wilcoxon because the pairs were unmatched, and the Wilcoxon test requires matched data ("Kruskal-Wallis and Friedman Tests" 2016). The Mann-Whitney U test is a simplified Kruskal-Wallis test, analyzing only two groups instead of multiple (McKight and Najab 2010). The Kruskal-Wallis was run first to determine if a Mann-Whitney should be applied to an individual group (i.e. phase of ENSO), then the Mann-Whitney was performed between each phase of ENSO. The Mann-Whitney is a measure of difference within mathematical space, or the difference in the location of the distribution.

Dissecting this first by season, the increase in tornado counts across ENSO phases during spring is apparent through Weak La Niña. As ENSO transitions from Moderate El Niño to Weak La Niña, the number of tornadoes increases from 250 to almost 450. To define the statistical significance of these differences in counts across ENSO phase, the Kruskal-Wallis (Table 2.1)

and Mann-Whitney tests were applied. Results for the Mann-Whitney test in spring are listed in Table 2.2.

Table 2.2: Mann-Whitney resulting p-values for spring (very strong evidence – pink; strong – orange; moderate – yellow; weak or none – dark grey; no data – light gray)

	Strong El Niño	Moderate El Niño	Weak El Niño	Neutral	Weak La Niña	Moderate La Niña	Strong La Niña
Strong El Niño							
Moderate El Niño		-	-	-	-	-	
Weak El Niño		0.0444	-	-	-	-	
Neutral		0.0021	< 0.001	-	-	-	
Weak La Niña		0.0440	0.6784	< 0.001	-	-	
Moderate La Niña		0.6667	0.2222	0.0465	0.1538	-	
Strong La Niña							

Figure 2.5 demonstrates that Moderate El Niño and Weak La Niña are very different from each other, and Mann-Whitney test verifies that with a significantly strong p-value of 0.0440. Moderate La Niña almost consistently results in a non-significant p-value. Box-and-whisker plots are examined (Figure 2.7) to better understand this result. The Mann-Whitney analysis and the box-and-whisker plot both reveal dissimilarity between Moderate La Niña and other phases (Figure 2.7B). However, Moderate La Niña only has one value, resulting in a distribution that is just a line, which could be the cause of non-significance. Therefore, it is important to note that spring MLN frequencies should not be trusted as much as other tornado frequencies in spring. Out of all the relationships between ENSO phases in the spring, six out of ten of them are significantly different from each other (Table 2.2).

(A) (B)

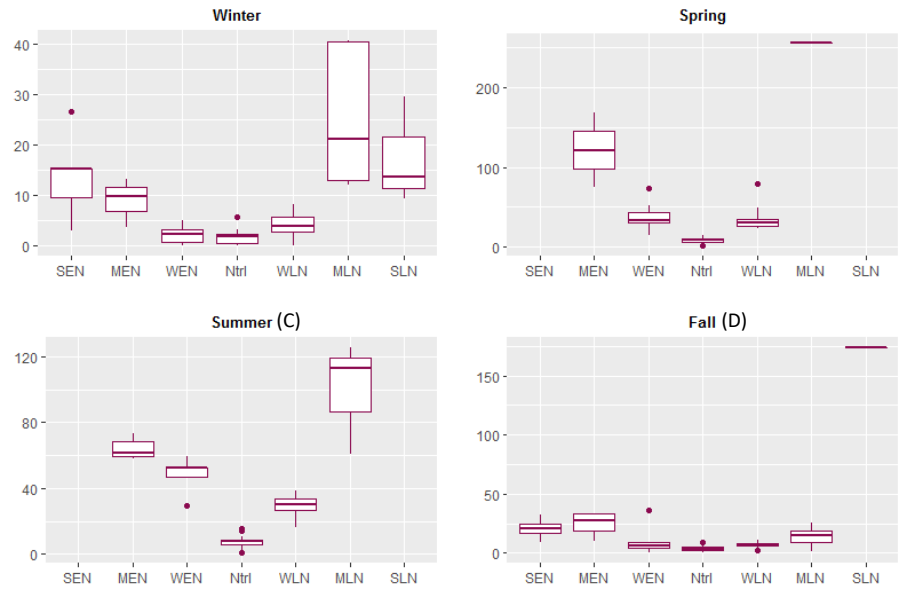

Figure 2.7: Box-and-whisker plots of tornado counts for winter (A), spring (B), summer (C), and fall (D) by ENSO phase

Looking across ENSO phases in summer (Figure 2.5), it seems that there is not much difference across the varying phases of ENSO, except for a drop in counts during Weak El Niño. However, Table 2.3 and Figure 2.7C indicate there is evidence for statistical differences between detrended tornado counts in most ENSO phases and intensities.

Table 2.3: Mann-Whitney resulting p-values for summer (very strong evidence – pink; strong – orange; moderate – yellow; weak or none – dark grey; no data – light gray)

	Strong El Niño	Moderate El Niño	Weak El Niño	Neutral	Weak La Niña	Moderate La Niña	Strong La Niña
Strong El Niño							
Moderate El Niño		-	-	-	-	-	
Weak El Niño		0.0159	-	-	-	-	
Neutral		< 0.001	< 0.001	-	-	-	
Weak La Niña		< 0.001	0.0133	< 0.001	-	-	
Moderate La Niña		0.2500	0.0357	< 0.001	0.0055	-	
Strong La Niña							

This implies that the distribution of tornado counts between varying phases of ENSO in summer are statistically different, though the average detrended annual count does not show the same. Fall and winter seasons demonstrate that tornado counts decrease dramatically when

changing from spring/summer (Figure 2.5). Strong La Niña has the greatest tornado count across all phases of ENSO in fall. However, Table 2.4 reports non-significant p-values between Strong La Niña and the remaining six ENSO phases, except for the neutral phase.

Table 2.4: Mann-Whitney resulting p-values for fall (very strong evidence – pink; strong – orange; moderate – yellow; weak or none – dark grey)

	Strong El Niño	Moderate El Niño	Weak El Niño	Neutral	Weak La Niña	Moderate La Niña	Strong La Niña
Strong El Niño	-	-	-	-	-	-	-
Moderate El Niño	0.4857	-	-	-	-	-	-
Weak El Niño	0.0418	0.0132	-	-	-	-	-
Neutral	< 0.001	< 0.001	0.0279	-	-	-	-
Weak La Niña	0.0103	< 0.001	0.3793	< 0.001	-	-	-
Moderate La Niña	0.3152	0.1636	0.0684	< 0.001	0.0346	-	-
Strong La Niña	0.4	0.4	0.1538	0.0741	0.1667	0.25	-

This is again because Strong La Niña only has one value, not a distribution, which could be the cause of non-significance (Figure 2.7D), and should be noted. There are fewer statistically significant pairings in fall than spring and summer, but there are more categories present due to all seven ENSO categories having tornado counts. Twelve out of 21 relationships in the fall are significantly different from each other (Table 2.4). Winter shows an interesting trend in tornado counts, with a "U" shape across ENSO phases and a large spike during Moderate La Niña (Figure 2.5). Strong El Niño has a large tornado count, which decreases dramatically across the other El Niño phases, then increases again through WLN and MLN. Table 2.5 shows evidence indicating paired groups that have statistical differences between each other (13 out of 21).

Table 2.5: Mann-Whitney resulting p-values for winter (very strong evidence – pink; strong – orange; moderate – yellow; weak or none – dark grey)

	Strong El Niño	Moderate El Niño	Weak El Niño	Neutral	Weak La Niña	Moderate La Niña	Strong La Niña
Strong El Niño	-	-	-	-	-	-	-
Moderate El Niño	0.5714	-	-	-	-	-	-
Weak El Niño	0.0025	0.0172	-	-	-	-	-
Neutral	< 0.001	< 0.001	0.4505	-	-	-	-
Weak La Niña	0.0194	0.1107	0.0137	< 0.001	-	-	-
Moderate La Niña	0.3095	0.1429	< 0.001	< 0.001	< 0.001	-	-
Strong La Niña	1.0	0.4	< 0.001	< 0.001	< 0.001	0.5714	-

Overall, 40 out of 62 pairings resulted in statistical significance, meaning that 64.5% of ENSO phases have significantly different tornado frequencies when compared against each other.

2.3.4 Atmospheric Composite Analysis

Seasonal composites of 500 hPa geopotential height, 850 hPa wind fields, and 300 hPa wind fields were analyzed to identify underlying atmospheric patterns that potentially contribute to shifts in tornado activity identified in Section 2.3.2. A geopotential height approximates the actual height of a pressure surface above mean sea-level (NOAA 2017). In this case, 500mb geopotential heights are the approximated height above mean sea-level at which the pressure is 500mb. Contours are used to show patterns of similar geopotential heights, resulting in ridges and troughs, which are indicative of circumpolar vortex variability (which can be influenced by ENSO, Frauenfeld and Davis 2003), location and intensity of jet streams, and locations of storm tracks over the U.S. Examining geopotential height anomalies, or departures from long-term means of geopotential height, is also useful in determining mid-level troughs and ridges, as well as zonal and meridional flows and resultant severe weather episodes. Negative anomalies tend to indicate storminess as cooler air aloft is advected atop a warmer airmass below (Drakoen 2008). For this analysis, anomaly data provided by the NCEP/NCAR Reanalysis was calculated as the departure from the climatology during 1981-2010 to match the new climate normal time period (ESRL 2016). Finally, because vertical wind shear is one of the most important components in severe weather and tornado occurrences (Brooks et al. 2003), winds at the 850mb level and 300mb level are also analyzed to exhibit deep-layer shear, as well as low-level advection. These atmospheric composites were retrieved from the NCEP/NCAR Reanalysis Dataset available via the Earth System Research Laboratory (ESRL) (Kalnay et al. 1996), and plotted in R (R Core Team 2016). This global dataset is defined on a 2.5° longitude by 2.5° latitude grid (Figure 2.8)

with 17 vertical levels, starting at 1000hPa.

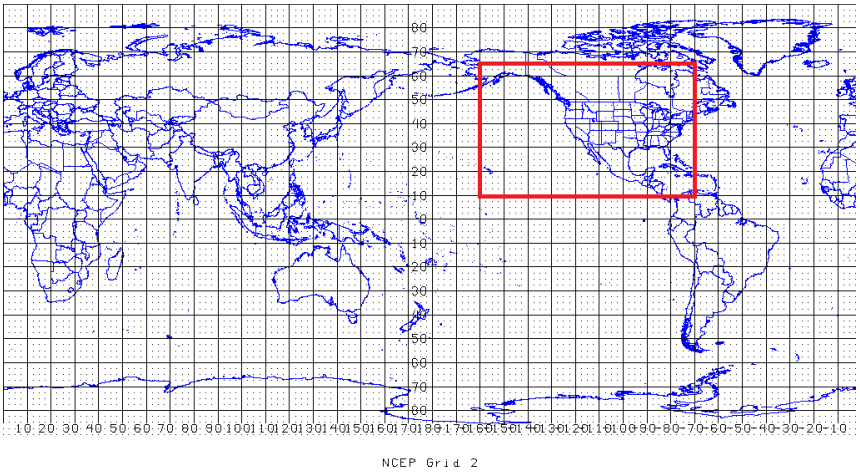

Figure 2.8: Domain used for NCEP/NCAR Renalaysis Data. Red rectangle indicates subdomain used for this study. Figure from http://www.nco.ncep.noaa.gov/pmb/docs/on388/tableb.html

Data was imported into R for each season and phase of ENSO, resulting in 24 separate NetCDF files per variable. World map countries and coastlines were downloaded from Natural Earth's large scale database ("Downloads, Natural Earth" 2016). To analyze atmospheric conditions over the United States as well as ENSO conditions over the eastern Pacific, a region encompassing 70°W to 160°W longitude and longitude and 10°N to 65°N latitude was chosen (shown in red in Figure 2.8). Although a total of 24 composite maps were developed, only plots most relevant to the analyses in Section 2.4 will be shown.

2.4 Discussion

Seasonally, winter and spring exhibit the strongest shifts in tornado activity, although fall exhibits an interesting change in frequency during SLN. Figure 2.5 shows a general increase in tornado counts as ENSO transitions from El Niño to La Niña phases in both seasons; summer shows little to no variation. Fall shows consistency in six of the seven phases, with a spike during the SLN phase. Geographically, Figure 2.3 shows a general northward expansion of hot

spots in winter as La Niña becomes stronger, while spring tornado hot spots typically shift eastward as ENSO changes from El Niño to La Niña. While tornado activity in most ENSO phases are not remarkably different from each other, the differences described above will be analyzed in this section. Atmospheric composites during summer will also be analyzed to confirm non-variability between ENSO phases.

In winter, MLN favors increased tornado activity. To understand the increase in tornado counts during a more intense La Niña phase, versus El Niño phases, the atmospheric composite for winter MEN and MLN will be compared (Figures 2.9A and 2.9B).

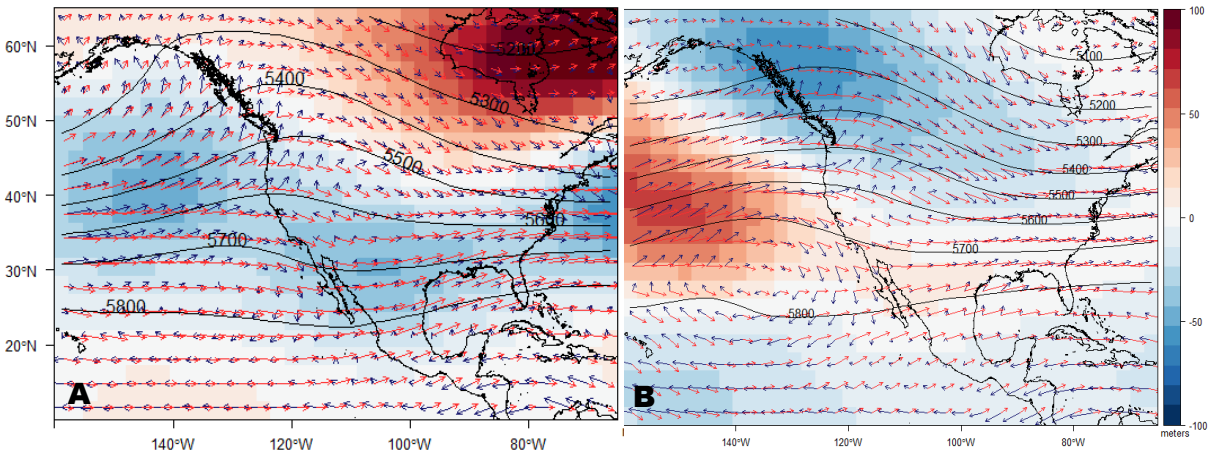

Figure 2.9: Atmospheric composites for Winter MEN (A) and Winter MLN (B). Contours represent 500hPa geopotential heights. Shading represents 500hPa geopotential height anomalies. 850hPa (300hPa) mean wind vectors are shown in blue (red).

Winter MLN composites exhibit a negative anomaly over western Canada/U.S., indicating low-level pressure to the east of the trough over the north-central U.S. (Figure 2.9B). Meridionally oriented low-level winds are also evident, which transport warm, moist low-level air of maritime tropical origin to inland areas. This creates an environment conducive for tornado activity, based on the Barnes and Newton (1986) diagram for typical synoptic conditions favorable for severe weather (Figure 2.10).

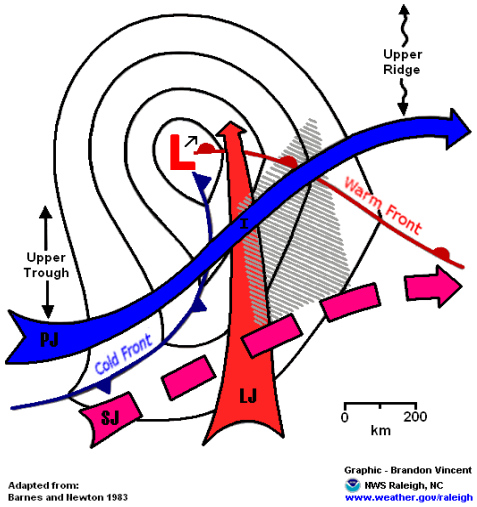

Figure 2.10: Typical synoptic conditions favorable for severe weather in the United States. Figure adapted from Barnes and Newton (1986).

MEN in winter (Figure 2.9A) exhibits negative geopotential height anomalies over the central U.S. This negative anomaly is consistent with a southwardly displaced surface cyclone track along the GOM identified in previous studies (Eichler and Higgins 2006) during El Niño events. Southeasterlies are advecting warm moisture over Florida, indicative of potential activity; however, the position of the low explains why there is a decrease in tornado activity, as well why tornadoes occur most frequently along the GOM during this phase. These results are consistent with previous findings (Cook and Schaefer 2008), as well as typical ENSO conditions during winter (CPC 2016). The lack of tornadic activity in Florida during other ENSO phases is likely due to a decrease in GOM cyclogenesis in these areas.

In spring, a WLN cultivates increased tornado activity. Hot spot analyses in Section 2.3.2 also reveal that this phase promotes eastward displacement of tornado hot spots when compared to El Niño phases. Composites comparing Spring WEN (Figure 2.11A) and Spring WLN (2.11B) verify increased tornado activity during La Niña phases.

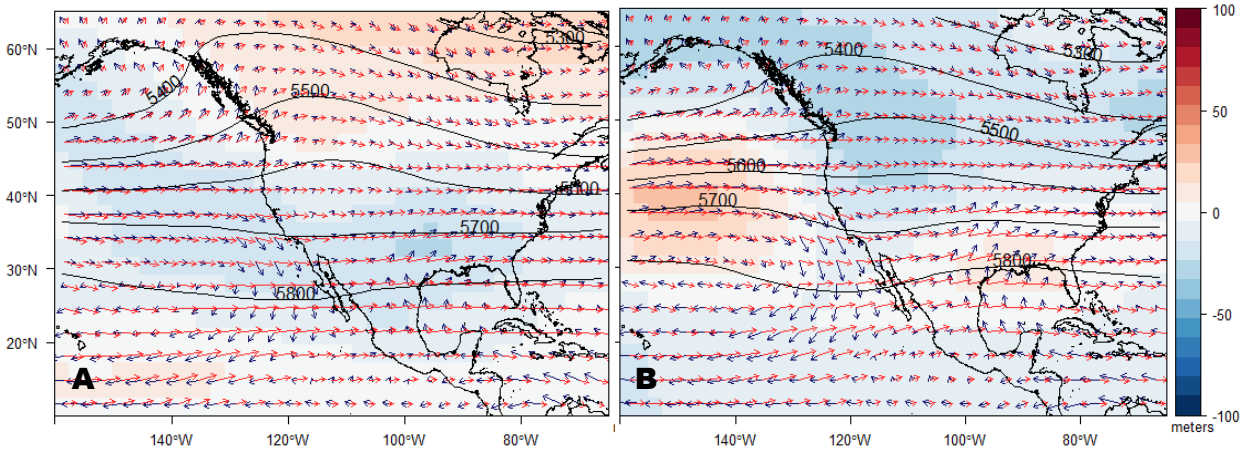

Figure 2.11: Atmospheric composites for Spring WEN (A) and Spring WLN (B). Contours represent 500hPa geopotential heights. Shading represents 500hPa geopotential height anomalies. 850hPa (300hPa) mean wind vectors are shown in blue (red).

In WEN, negative anomalies of geopotential height exist across much of the southern tier of the U.S. (Figure 2.11A). This is consistent with a southwardly displaced surface cyclone track (as shown in Figure 2.3J) over much of the U.S. Meridionally oriented low-level winds are advecting tropical moisture from the GOM, which is conducive for tornado activity; however, the position of the mid-level height anomalies would foster more tornado activity along the southern U.S. compared to its WLN counterpart (Figure 2.11B), where broader warm sectors can make more inland progress and foster tornado activity at higher latitudes. During a WLN, a negative anomaly over the northwestern U.S. typically indicates areas of low-pressure at the surface over the central U.S. (Figure 2.11B), which in turn aids in southerly flow at 850 hPa (also shown in Figure 2.11B) and more frequent moisture influxes from the Gulf of Mexico, resulting in greater tornado activity (Figure 2.3R, Figure 2.5). Aside from increased tornado frequency, an eastward expansion of hot spots from El Niño to La Niña is an important finding in this study. It is hypothesized that the expansion of tornado hot spots further eastward during La Niña phases (Figure 2.11B) compared to El Niño phases (Figure 2.11A) is due to increased low-level meridional winds during WLN (Figure 2.11B), which could potentially be advecting more

moisture across the southern plains and enhancing tornado activity. These atmospheric parameters explain both the increase in tornado activity during Spring WLN as well as an eastward expansion in hot spots when compared to El Niño phases.

The influence of ENSO on tornado activity in summer is generally weak compared to other seasons, resulting in little variation in average annual tornado frequencies between ENSO phases. Hot spots also show little variation in geographic location across all five phases, which is consistent with the northward displacement of the jet stream (Frauenfeld and Davis 2003) and tornadic activity (Brooks et al. 2003) during summer compared to other seasons. Summer MLN and summer WEN composites (Figures 2.12A and 2.12B) exhibit very similar mean atmospheric conditions, which also confirms the similarities in observed tornado hot spots and average annual frequency shown in Section 2.3.

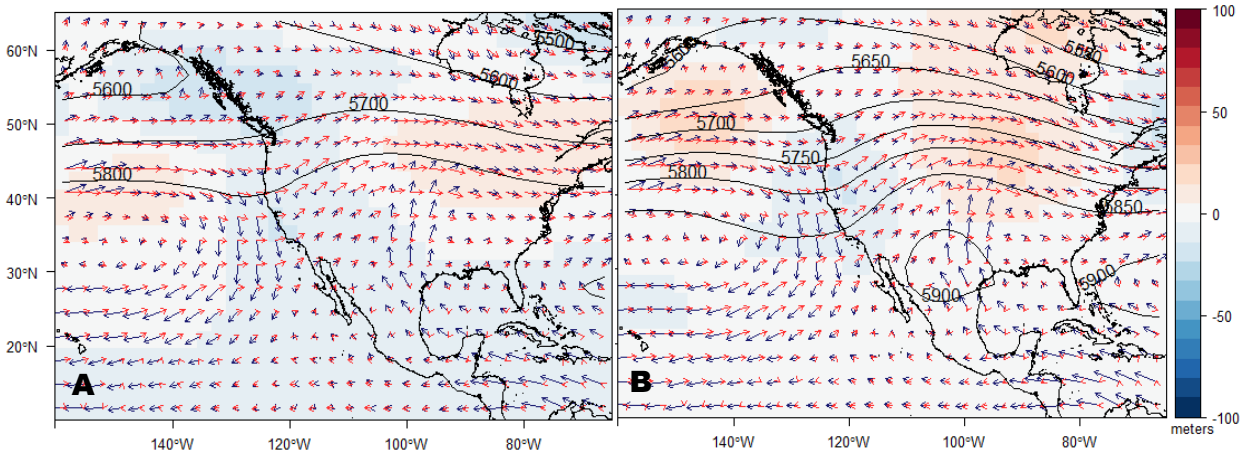

Figure 2.12: Atmospheric composites for Summer MLN (A) and Summer WEN (B). Contours represent 500hPa geopotential heights. Shading represents 500hPa geopotential height anomalies. 850hPa (300hPa) mean wind vectors are shown in blue (red).

Both summer MLN (Figure 2.12A) and WEN (Figure 2.12B) composites exhibit a northwardly displaced jet stream, with a trough over the west coast. Strong southerly winds are advecting warm, moist air from the GOM leading to increased potential for severe weather over

the central U.S. Persistent negative height anomalies in both MLN and WEN composites along the west coast of the U.S. reinforces the notion that ENSO exhibits little influence on severe weather activity in the eastern U.S. during summer.

Fall SLN tends to foster increased tornado activity, while the other six phases of ENSO have a smaller effect. Fall SLN is compared to a fall SEN phase to understand why there is an increase in counts during this phase (Figures 2.13A and 2.13B).

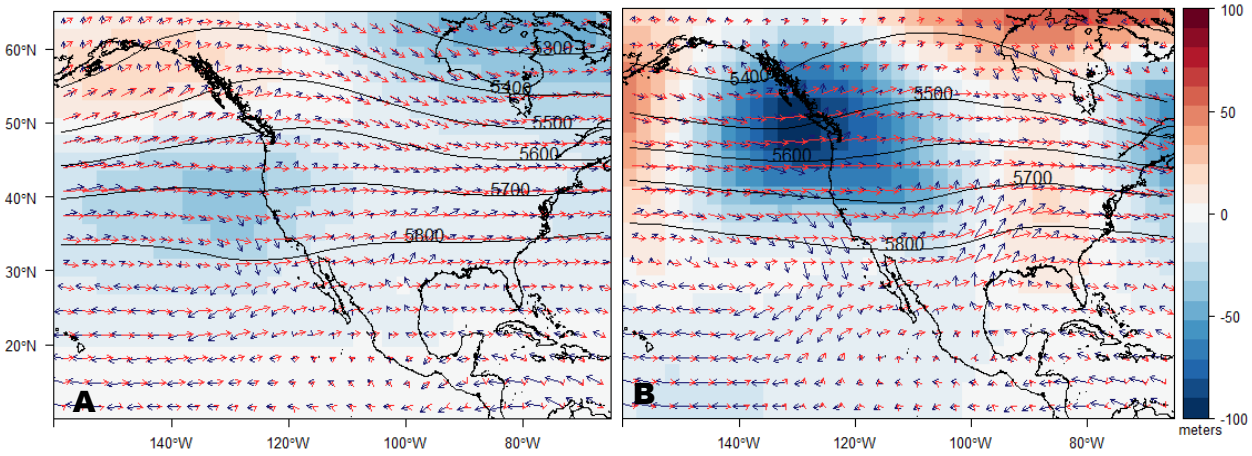

Figure 2.13: Atmospheric composites for Fall SEN (A) and Fall SLN (B). 850hPa (300hPa) wind vectors are shown in blue (red). Contours represent 500hPa geopotential heights. Shading represents 500hPa geopotential height anomalies. 850hPa (300hPa) mean wind vectors are shown in blue (red).

Atmospheric conditions during SLN in fall are more favorable for tornado activity than in other ENSO phases. The SEN composite exhibits a "split-flow" pattern, where the subtropical jet is positioned over the southern U.S. and a polar jet is oriented from central Canada southeastward into the northern states (Figure 2.13A). Generally, negative anomalies over Hudson Bay can be inhibitive of tornado activity inland due to low-level cold air surges from Canada. This is indicated by mean northwesterly 850 hPa wind fields. On the other hand, SLN has a large magnitude negative anomaly over western Canada, and a positive anomaly over the eastern U.S northward near Hudson Bay (Figure 2.13B). These features generally favor low-

level warm/moist advection indicated by the 850 hPa flow, which generally fosters increased tornado activity during these phases. Differences in 850 hPa flow between the two phases might also explain the variability in tornado activity between the two – there is a large increase in 850hPa winds during a SLN phase compared to a SEN phase, which is conducive for tornado activity. However, this large increase in annual frequency during SLN is not reflected in the hot spots (Figure 2.3AB). The lack of hot spots present is likely due to a sample size issue, which was found with non-significant Mann-Whitney results when compared to other ENSO phases in fall. Though the SLN composite indicates generally favorable synoptic-scale conditions for tornado activity, the increase in tornado counts during these phases should has a lower confidence compared to other phases during this season.

Winter and spring exhibit the largest ENSO-related spatial shifts in tornado activity. During winter El Niño, tornado activity is displaced southward along the GOM, while a general northward displacement of activity is observed during La Niña phases. These findings are consistent with Cook and Schaefer (2008). Tornado frequency is highest in winter during MLN conditions in the equatorial Pacific, although a general increase in tornado counts is evident with progressively cooler sea surface temperatures. In spring, as ENSO transitions from El Niño to La Niña phases, a general eastward expansion of tornado activity across the Central Plains is evident in the hot spots, which is likely due to increased low-level winds advecting more moisture across the southern plains (Figure 2.11B). Out of the four seasons, spring WLN has the largest tornado count. Summer shows little variation both spatially and in annual tornado frequencies. Fall shows slight variation across ENSO phases, but the geographic distribution of hot spots is sporadic and does not follow a specific pattern. There is an apparent increase in frequency during Strong La Niña, but a sample size of one in the box-and-whisker plots resulted in non-significant

p-values to validate this observation.

To better visualize the differences in tornado hot spots between each phase of ENSO during a particular season, difference maps were created and are shown below (Figures 2.14 and 2.15). The colored grid cells exhibit a cell that has a hot spot only in the respective phase of ENSO, which are referred to as “unique hot spots”.

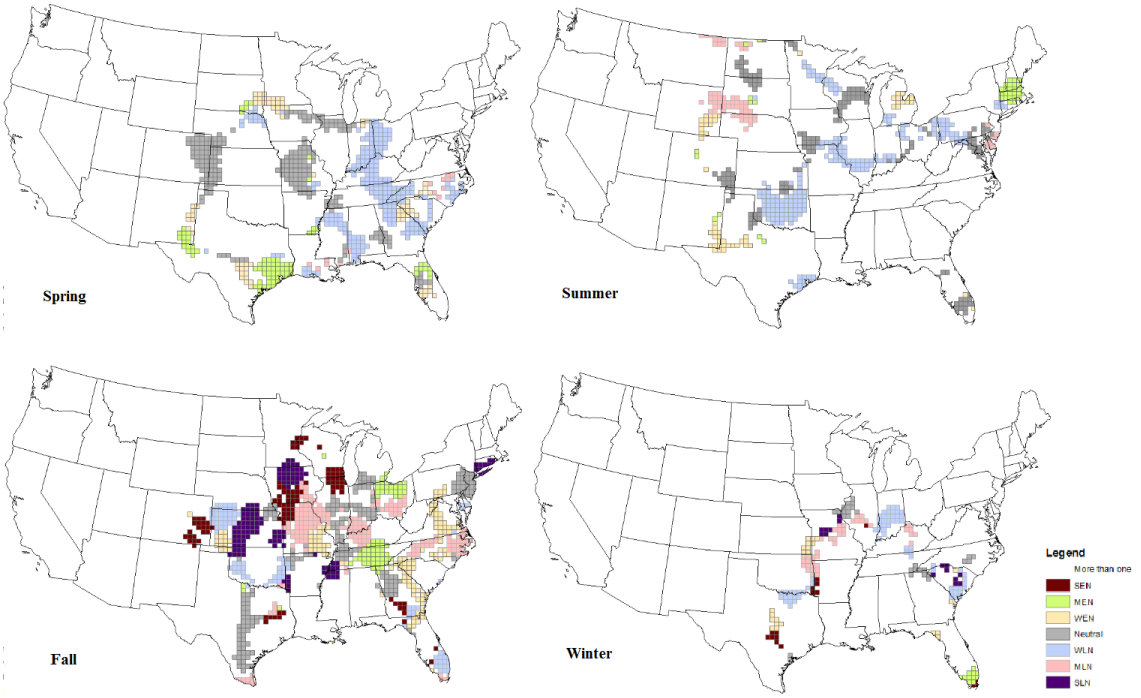

Figure 2.14: Unique hot spots across seven phases of ENSO for all seasons, 1950-2014

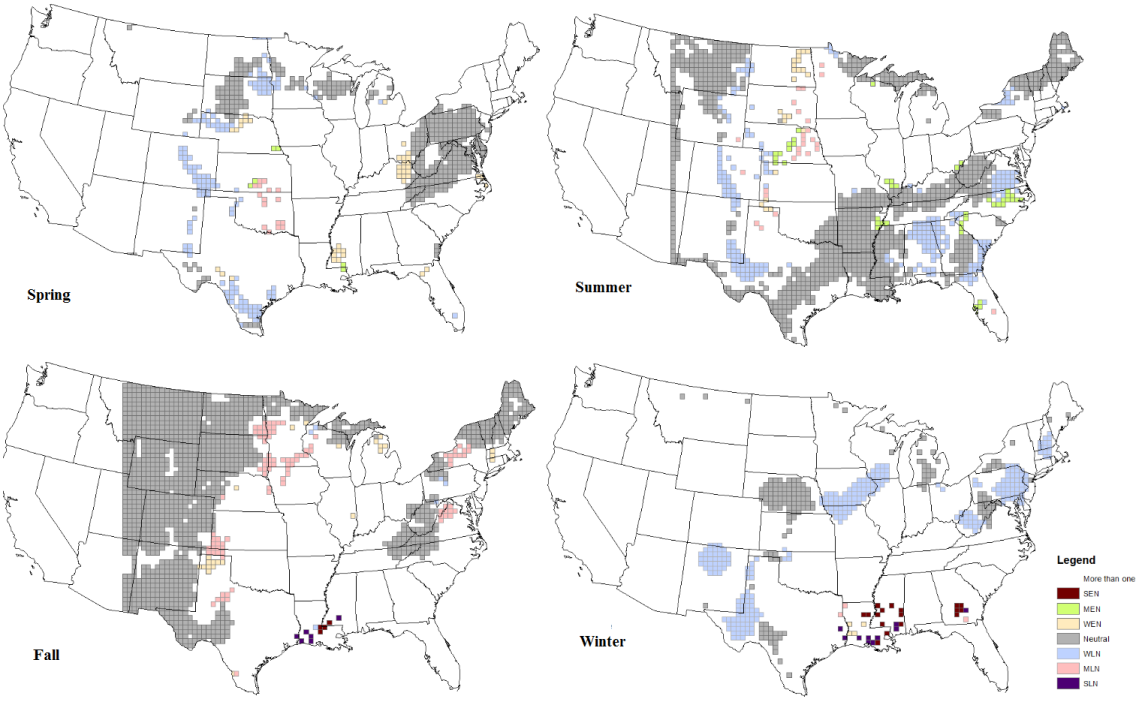

Figure 2.15: Unique cold spots across seven phases of ENSO for all seasons, 1950-2014

Figure 2.14 visualizes the geographic shift in hot spots across all four seasons. In spring, as ENSO transitions from El Niño to La Niña, hot spots move from a Midwestern location further eastward – this is visible in Figure 2.3. Unique hot spots during WLN are visible across parts of Dixie Alley and extending northward into Indiana and Ohio, and unique MEN hot spots are evident along the Texas coastline, indicating an eastward shift from El Niño to La Niña. The potential cause of this could be due to an increase in 850 hPa winds, increasing low-level moisture advection from the GOM during WLN compared to WEN. In fall, the inconsistent hot spots are visible in Figure 2.3, where there is no evident pattern between the phases of ENSO, which is verified by a wide variety of unique hot spots. Also, due to some hot spots in particular phases being adjacent to hot spots of an opposite ENSO phase (i.e. SEN right next to SLN), it is difficult to say with certainty that there is an ENSO influence in these regions. Winter shows a northward expansion of hot spots when transitioning from El Niño to La Niña, and this is evident in Figure 2.3. with unique hot spots during WLN and MLN along the north Central Plains. The

northward displacement of the jet stream seen in Figure 2.9B during MLN exhibits why unique hot spots belong to stronger La Niña phases.

Figure 2.15 shows mostly unique cold spots in the Neutral phase due to the presence of cold spots during this phase with respect to the other phases, but WLN also has some unique cold spots during spring, summer and winter.

2.5 Conclusion

Tornadoes from 1950 through 2014 were analyzed geographically to determine potential influences from ENSO. A seasonal Niño 3.4 index was derived from the original Niño 3.4 index to better represent tornadic activity seasonally without involving a running 3-month mean (like the ONI). Annual tornado counts were detrended to remove the uptick that has been observed in tornado counts due to urbanization, technology improvements, and population increase. Spatial statistics such as the Average Nearest Neighbor and Global Moran's I were performed to confirm spatial clustering, then local statistics (Optimized Hot Spots) were applied to visualize where spatial clustering was happening across the study region. It was found that in spring, a Weak La Niña phase means more tornadoes on average (Figure 2.5). Hot spots persistently lie over the central U.S. in spring, and expand eastward as ENSO transitions from El Niño to La Niña. A weaker La Niña phase indicates more tornadoes annually as well as a larger spatial region of significant hot spots in spring. Summer has a relatively even distribution of tornado counts across ENSO phase, with Weak El Niño showing smaller annual frequency than the other phases of ENSO. Spatially, summer has little change geographically, with decreases in hot spots likely occurring as a dampening in sample size. Fall has its largest tornado count during a Strong La Niña, very little difference in annual counts in the remaining six fall ENSO phases. However, due to a sample size of one for Strong La Niña (Figure 2.7), the Mann-Whitney test returned

non-significant results when tested against other ENSO categories during fall (Table 2.4). Geographic distribution in fall does not show changing patterns across ENSO phases, however El Niño phases seem to have more aggregated hot spots while La Niña phases are more dispersed. This is verified by global spatial statistics, which indicate stronger clustering during El Niño phases and weaker clustering during La Niña phases. Winter also shows tendency for higher tornado counts during La Niña phases, except for a Strong El Niño phase. A relatively large hot spot extent along the Gulf and Central Plains zones during Strong El Niño might be the cause of this spike in annual tornado frequency, which could be the result of outbreak(s) during winter. As ENSO transitions from El Niño to La Niña in winter, hot spots grow and extend further north with the exception of Strong La Niña. This is largely due to the position of the jet stream as well as persistent troughing in the northwestern U.S./Canada in La Niña phases. The statistical differences between adjusted tornado counts across ENSO phases were tested using the Mann-Whitney test, and 40 out of 62 individual relationships between two groups (64.5%) resulted as statistically different (Tables 2.2 through 2.5). This means that the intensity of ENSO does have an impact on tornado frequencies, but a spatial analysis is vital to fully understand its influence. Overall, results of this study conclude that the intensity of ENSO does have an influence on tornadoes in the eastern United States. ENSO influences spatial distribution in all phases of ENSO, and tornado frequencies generally tend to be higher during La Niña phases. A larger sample size would be beneficial to the moderate and strong phases of El Niño and La Niña; future studies could improve this type of study with a longer time period to resolve this issue. Future research could utilize the seasonal findings of this study through machine-based learning to create a functional prediction tool, which has been studied previously but only for spring (LaCorte 2011).

CHAPTER 3: THE INFLUENCE OF ENSO ON WEAK AND STRONG TORNADOES IN THE EASTERN UNITED STATES

3.1 Introduction

The record-breaking tornado outbreak in spring 2011 caused 1084 tornadoes, 5,182 injuries, 541 deaths and over $9 trillion in estimated property losses (Lee et al. 2013; SPC 2016). During this time, the eastern Pacific was transitioning from a Moderate La Niña to a Weak La Niña, raising questions as to whether this teleconnection was linked to the massive tornado outbreak. (Lee et al. 2013). Previous studies have shown a connection between ENSO (specifically La Niña phases) and tornado activity in the eastern United States (Monfredo 1999; Marzban and Schaefer 2001; Lee et al 2013; Allen et al. 2015; Lee et al. 2016), but no studies have analyzed the role that the intensity of ENSO plays.

This chapter aims to discover characteristics of the tornado-ENSO intensity relationship as it is related to tornado intensity, tornado days, and the Destruction Potential Index (DPI) (Thompson and Vescio 1998). While previous studies have analyzed seasonal tornado frequency and geographic distribution as a function of ENSO (Bove 1998; Schaefer and Edwards 1999; Marzban and Schaefer 2001; Cook and Schaefer 2008; Lee et al. 2013; Allen et al. 2015), no studies have analyzed the relationship as a function of ENSO intensity as well. Of these studies, very few have analyzed the influence ENSO has on tornado intensity and tornado days (Cook and Schaefer 2008; Lee et al. 2013). Understanding the geographical variability of tornadoes by tornado intensity as a function of ENSO could potentially result in improved seasonal forecasts for such activity in the United States. Analyzing tornado days as a function of ENSO would also benefit seasonal outlooks by preparing for tornado outbreaks during a specific phase. This chapter examines the spatial distribution and temporal change in tornado frequency and

distribution for “weak” (EF-0 and EF-1) and “strong” (EF-2 through EF-5) tornadoes on the EF-scale from 1950 through 2014. The statistical significance of both spatial and temporal trends will be analyzed for confidence. As such, the objectives of this research are to:

1. To analyze tornado frequencies for weak and strong tornadoes as they relate to intensities of ENSO
2. To analyze the seasonality of weak and strong tornadoes across the eastern United States
3. To analyze the geographical distribution of tornadoes as related to ENSO
4. Analyze tornado days as a function of ENSO to better understand tornado outbreaks
5. Analyze trends in the Destruction Potential Index as a function of ENSO to better understand track area (i.e. length/width) during varying phases

3.2 Data

Various definitions of ENSO have been utilized when examining ENSO and tornadoes, such as the Trans-Niño Index (Lee et al. 2013), the Climate Prediction Center’s definition (Marzban and Schaefer 2001; Cook and Schaefer 2008), the Japan Meteorological Agency Index (Bove 1998), and the Oceanic Niño Index (Cook and Schaefer 2008). Cook and Schaefer (2008) also used a “4-tier” classification system to identify tornado outbreaks, and found that the definition of ENSO did not change the results by much. The Oceanic Niño Index (ONI), used recently by Allen et al. (2015), was stratified into a useful list of ENSO intensities by Golden Gate Weather Services (Null 2016). The ONI is a running 3-month mean of SST anomalies in the Niño 3.4 region. The thresholds to stratify phases of ENSO by intensity are positive for El Niño, and negative for La Niña. For example, SST anomalies for moderate La Niña would fall between -1.0 and -1.4. The intensities of ENSO are categorized under the following magnitudes:

- Weak: 0.5 - 0.9
- Moderate: 1.0 - 1.4
- Strong: Equal to or larger than 1.5

However, since this analysis evaluates tornadic activity by season, this averaging method would not reflect tornado relationships in a given season most effectively, as it would include values in the months surrounding the season. Therefore, a seasonal Niño 3.4 index was used. This seasonal index is an improvement of the ONI, specifically for this study, due to the seasonal categorization of ENSO intensity. Seasons were averaged and categorized over the following months: Winter (DJF), Spring (MAM), Summer (JJA), and Fall (SON). Data were retrieved from the Climate Prediction Center's Monthly Atmospheric and SST Indices database (CPC 2016). The monthly Extended Reconstructed SST (ERSSTv4) anomaly dataset with centered base periods was used because of its use in the ONI (CPC 2016), as well as its detrended mean for producing SST anomalies. A centered SST dataset was chosen as opposed to one with a 1981-2010 base period because this analysis began in 1950. Centered base periods detrend SST anomalies so that external variables such as climate change or an increase in SSTs are not an influence. With a 1981-2010 base period for an analysis starting in 1950, the adjusted SST average for a year early in the record (i.e. 1950) would be much warmer than what was observed from the increase in SSTs, indicating a higher mean for that year and resulting in a higher anomaly. Since the Niño 3.4 index values are an average SST anomaly value similar to the ONI, the same intensity thresholds from the ONI were used. It is noted that averaging SST values over a season pulls the distribution away from the extremes and towards weaker ENSO and neutral phases. Each season was binned into a Strong El Niño (SEN), Moderate El Niño (MEN), Weak El Niño (WEN), Neutral, Weak La Niña (WLN), Moderate La Niña (MLN), or Strong La Niña

(SLN) category based on its 3-month average SST anomaly value. A complete list of seasonally binned years for each ENSO phase are in the Appendix.

The Storm Prediction Center's Tornado Database provided the critical information necessary for this study (Schaefer et al. 1980; Schaefer and Edwards 1999). For the tornado intensity analysis, tornadoes were stratified into two categories. "Weak" tornadoes are tornadoes classified as either EF-0 or EF-1, and will be referred to as EF01. "Strong" tornadoes are the remaining EF-2 through EF-5 tornadoes, and are noted as EF25 in this study. Tornado start points, which were originally imported in a WGS84 coordinate system, were projected into a Lambert Conformal Conic projection. This projection was utilized because it is one of the best for mid-latitudes (ESRI 2016), where the study area is located. A conic projection was chosen as it starts at a single point over the poles and extends southward in a cone shape. This projection works best for all areas that have a greater east-west extent, like the United States (ESRI 2016). The Lambert Conformal was chosen over other conic projections, such as Albers, because it portrays shape more accurately than area which was desired for this study. A 40km grid is used as the grid of choice when analyzing count data due to its extensive use by the SPC (SPC 2016; Figure 3.1). The number of tornado touchdowns in each 40km grid cell were tabulated and used as the primary data source in this analysis

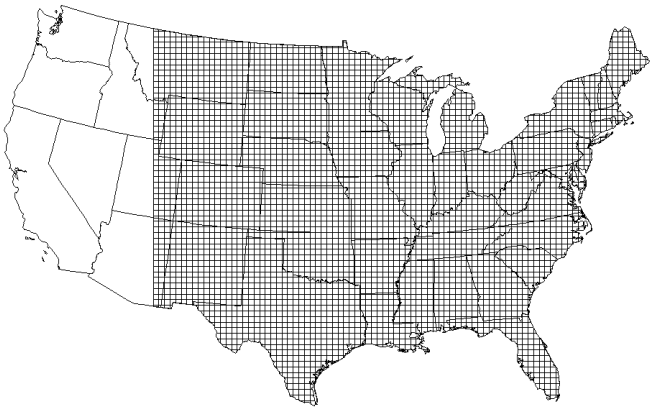

Figure 3.1. A 40-km grid depicting the study region chosen for this study.

To quantify tornadic intensity, the Destruction Potential Index is used as a measure of the potential for damage and causalities within an outbreak to examine the influence that ENSO has on tornado days, tornado strength and track area (Cook and Schaefer 2008). The equation is shown below, and further explained in section 3.3.4.

$$DPI = \Sigma [A_n (F_n + 1)] \quad \textbf{3.1}$$

Lastly, composites of mean atmospheric conditions during each ENSO phase were analyzed to better understand shifts in those conditions during varying phases and intensities of ENSO and their relationship with tornado counts, spatial distribution for weak and strong tornadoes, and tornado days. 500hPa geopotential height contours, 500hPa geopotential height anomalies, 850hPa wind vectors and 300hPa wind vectors were plotted Using data from ESRL's Monthly and Seasonal Climate Composites (ESRL 2016) for each season and phase/intensity of ENSO.

3.3 Methods and Results

3.3.1 Spatial Statistics Indicators

To determine whether there is evidence of spatial association in tornado incidents, two global indices of spatial autocorrelation were calculated: average nearest neighbor and global Moran's I. Average Nearest Neighbor calculates a nearest neighbor index based on the average

distance from each feature to its nearest neighboring feature (ESRI 2016). A random pattern generated from the Poisson process is compared against the real data to measure the strength of clustering. The null hypothesis is that the two processes are similar, or that there is no clustering and the features are randomly distributed. This tool was implemented on each season per ENSO category, resulting in a total of 24 statistical outputs based on available data per tornado intensity. The results are below in Figure 3.2.

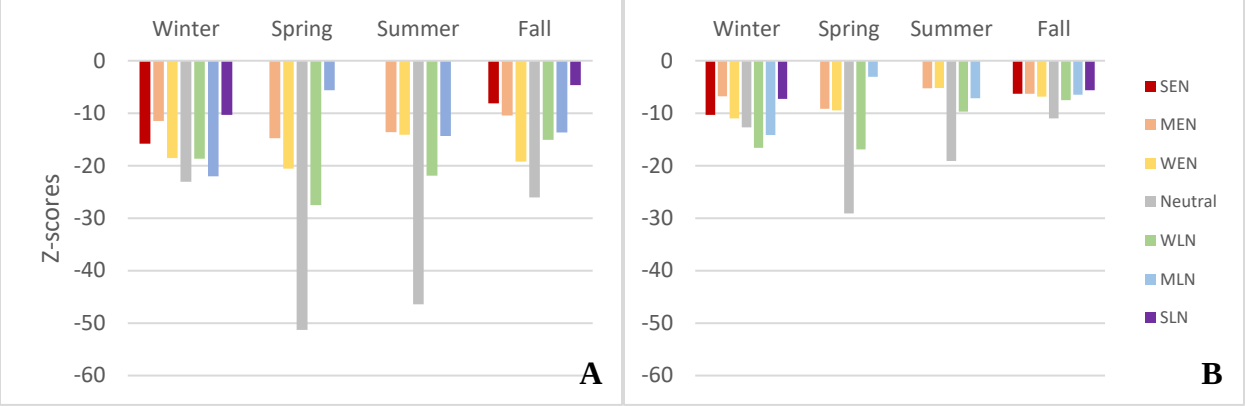

Figure 3.2. Average nearest neighbor z-scores across phases of ENSO for weak (A) and strong (B) tornadoes

The other tool, Global Moran's I, was used to verify and support spatial clustering through a different method. Given a set of features (i.e. tornado touchdown points) and an associated attribute (count data), this tool evaluates whether the pattern expressed is clustered, dispersed, or random (ESRI 2016). The associated attribute (count data) is derived from the number of points assigned to each cell in the 40km grid, resulting in a "count" number per fishnet grid. Again, the null hypothesis states that the values associated with the features are randomly distributed. For both analyses, z-scores were used to compare across phases and intensities of ENSO to determine which category has the strongest spatial clustering. Results also indicate if z-scores are similar or different, thereby determining which phases/intensities of ENSO have the largest effect on spatial autocorrelation amongst tornado counts. Figure 3.3

shows the z-scores for the Global Moran's I analysis. It should be noted that winter Moderate El Niño does not have a resulting z-score with Global Moran's I because it only had 28 tornadoes that classified as EF-2 through EF-5, and the GIS tool will not perform with less than 30 points (ESRI 2016).

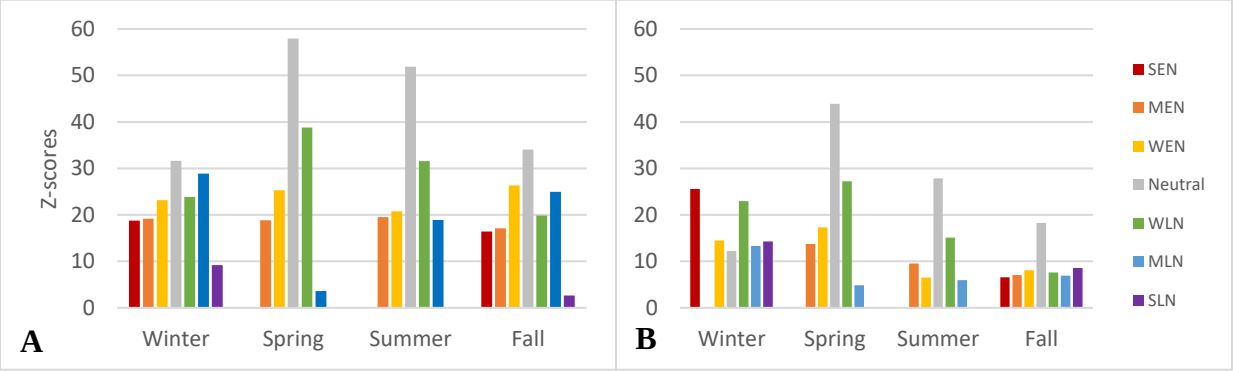

Figure 3.3: Global Moran's degree of spatial clustering for weak (A) and strong (B) tornadoes

For EF01 and EF25 tornadoes, all groups produced a significant p-value, rejecting the null hypothesis that the features are randomly distributed (i.e. no clustering). This was for all tornadoes with available F/EF-scale ratings in the record. It should be noted that out of the entire record, 55 tornadoes (.097%) did not have available F/EF-scale ratings and were not included in this analysis. Because all groups were statistically significant, z-scores can be compared to understand spatial clustering; a larger absolute value indicates stronger clustering. Spring and summer SEN and SLN had zero tornado counts and had no results in this analysis. EF01 tornado clustering (Figure 3.2A and 3.3A) strongly resembles clustering in all tornadoes (Figure 3.4), apart from slightly stronger clustering during winter WLN for all tornadoes.

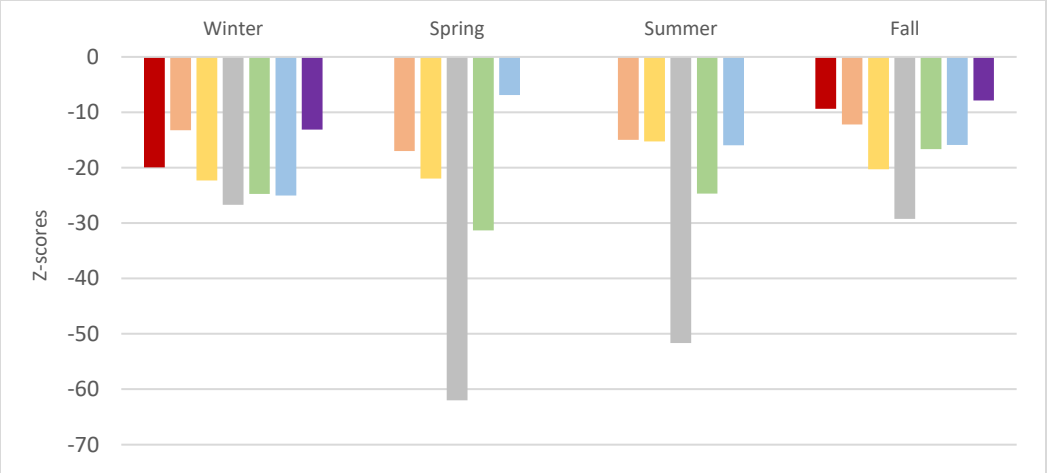

Figure 3.4. Average nearest neighbor z-scores across phases of ENSO for all tornadoes

EF25 tornadoes (Figure 3.2B and Figure 3.3B) show different patterns than all tornadoes (Figure 3.4) and EF01 tornadoes (Figure 3.2A and 3.2A). First, the strength of the clustering is weaker in EF25 tornadoes. This is most likely due to a smaller tornado count, meaning they are more geographically dispersed. However, the distribution of z-scores across seasons also changes, primarily in winter and fall. Spring and summer EF25 tornadoes both resemble a distribution similar to EF01 and all tornadoes, with a general increase in z-score from El Niño to La Niña and a dramatic decrease during MLN (this does not include the Neutral phase spike). However, strong tornadoes show the fall season having a relatively similar degree of spatial clustering throughout each phase of ENSO, except for a spike during the neutral season. This is unlike EF01 and all tornadoes, which resemble more of a bell-shape distribution of z-scores. This means that spatial clustering of EF25 tornadoes is generally independent of non-neutral ENSO phases during fall. In winter, the pattern itself remains similar to EF01 and all tornadoes, however the largest z-score belongs to the WLN phase instead of the Neutral phase. In fact, the z-score for WLN during winter and spring is almost identical. Spring MLN has the smallest spatial clustering, which is likely due to a small sample size.

3.3.2 Seasonal Hot Spots

Seasonal hot spot maps were created in GIS through the "Optimized Hot Spot Analysis" tool. Given incident points (i.e. tornado touchdown locations), this tool creates a map of statistically significant hot and cold spots using the Getis-Ord Gi* statistic (Getis and Ord 1992; ESRI 2016). Getis-Ord Gi* examines each feature within the context of neighboring features, or nearby tornado origin points. The local sum for a feature and its neighbors is compared proportionally to the sum of all features. When the local sum is much different than the expected local sum, and the difference is too large to have resulted from random change, it is scored a statistically significant Z-score (Mitchell 2005). For statistically significant (p-value less than or equal to 0.05) and positive Z-scores, a larger Z-score indicates more intense clustering of high values (hot spots). For statistically significant and negative z-scores, a smaller z-score indicates more intense clustering of lower values, or cold spots (ESRI 2016). Equations used in this statistic are accessible on ESRI's "Optimized Hot Spot Analysis" page (ESRI 2016).

GIS has two hot spot tools of choice – the standard Hot Spot Analysis (Getis_Ord Gi*), as well as the Optimized Hot Spot Analysis tool. For the purpose of this study, the latter method was utilized for several reasons. The Optimized Hot Spot tool automatically aggregates incident data, identifies appropriate scale of analysis, and corrects for both multiple testing and spatial dependence (ESRI 2016). The automatic aggregation of data allowed the input data features to be the original Conformal Lambert Conic projected tornado touchdown points. Most importantly, it identifies statistically significant spatial clusters of hot and cold spots, which are used in this study to identify local tornado clusters as a function of ENSO intensity and phase.

Figures 3.5 and 3.6 show plots representing ENSO hot spots across all seasons for EF01 and EF25 tornadoes, resulting in a total of 56 individual figures (nine of which have no

tornadoes). Figure 3.7 displays tornado hot spots for all tornadoes, for comparison against EF01 and EF25 tornado hot spots.

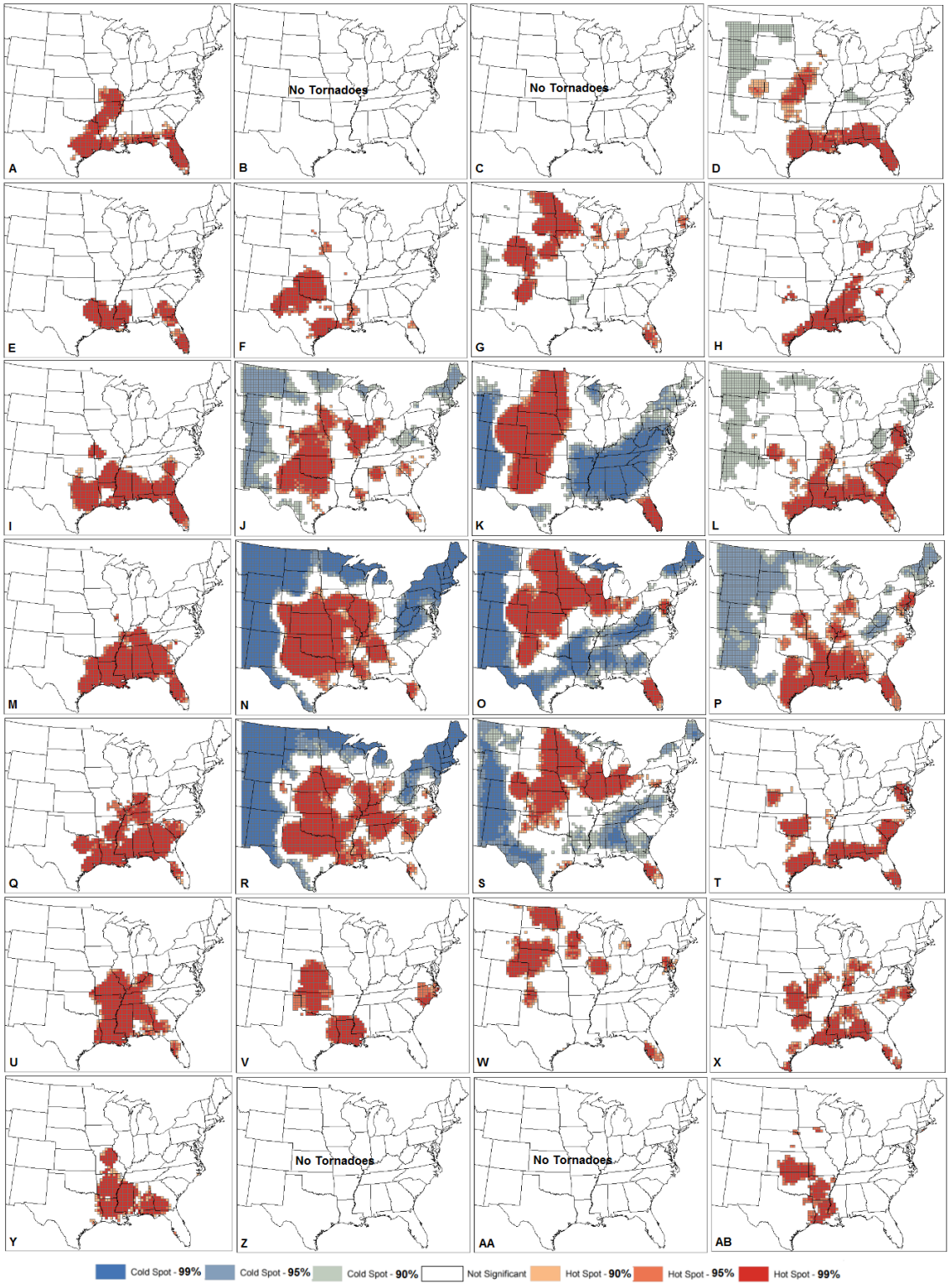

Figure 3.5: Weak (EF01) tornado hot and cold spots, 1950-2014. Columns are in the order of winter, spring, summer and fall. A-D are Strong El Niño, E through H are Moderate El Niño, I through L are Weak El Niño, M through P are Neutral, Q through T are Weak La Niña, U through X are Moderate La Niña, and Y through AB are Strong La Niña.

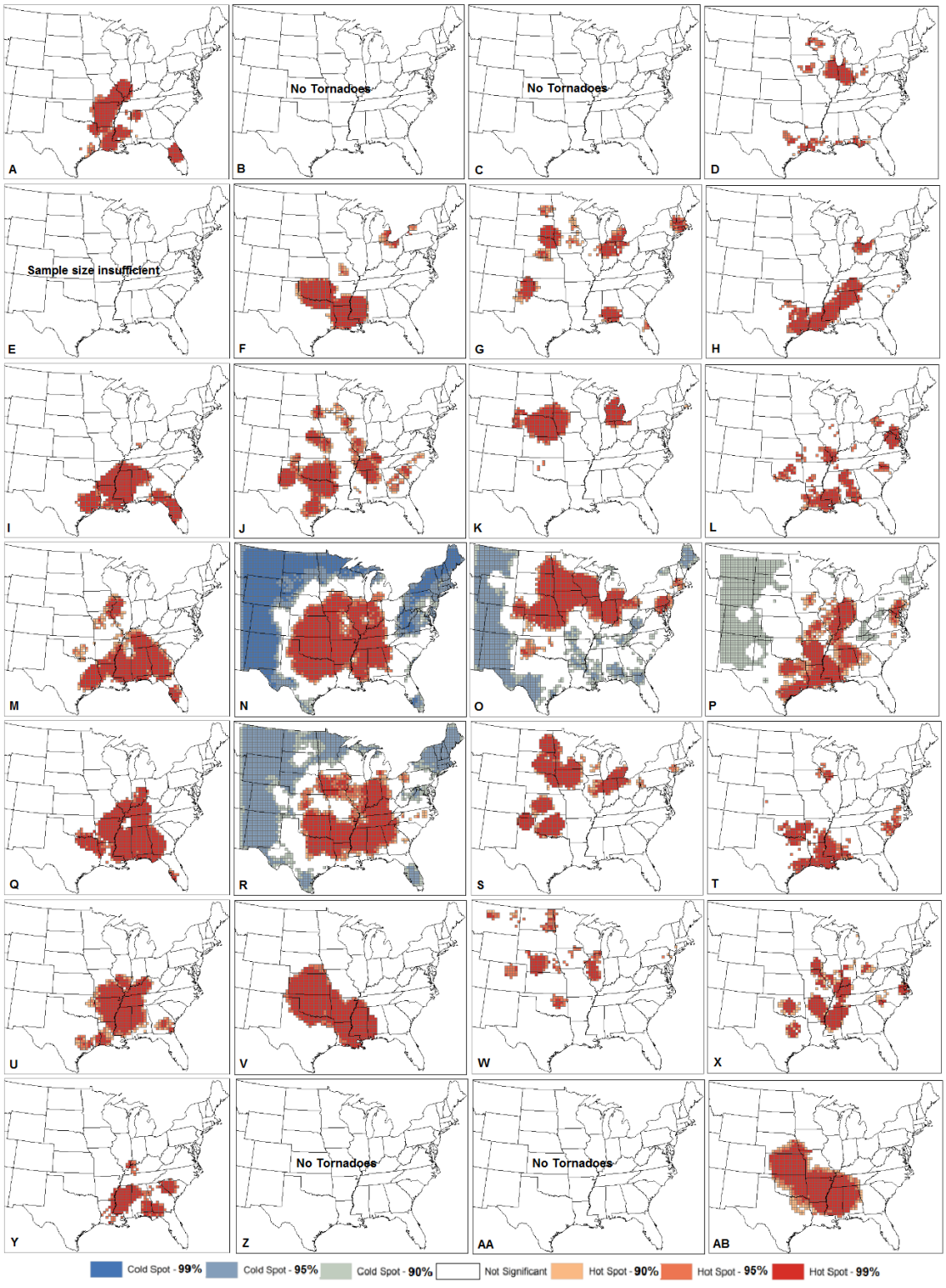

Figure 3.6: Strong (EF25) tornado hot and cold spots, 1950-2014. Columns are in the order of winter, spring, summer and fall. A-D are Strong El Niño, E through H are Moderate El Niño, I through L are Weak El Niño, M through P are Neutral, Q through T are Weak La Niña, U through X are Moderate La Niña, and Y through AB are Strong La Niña.

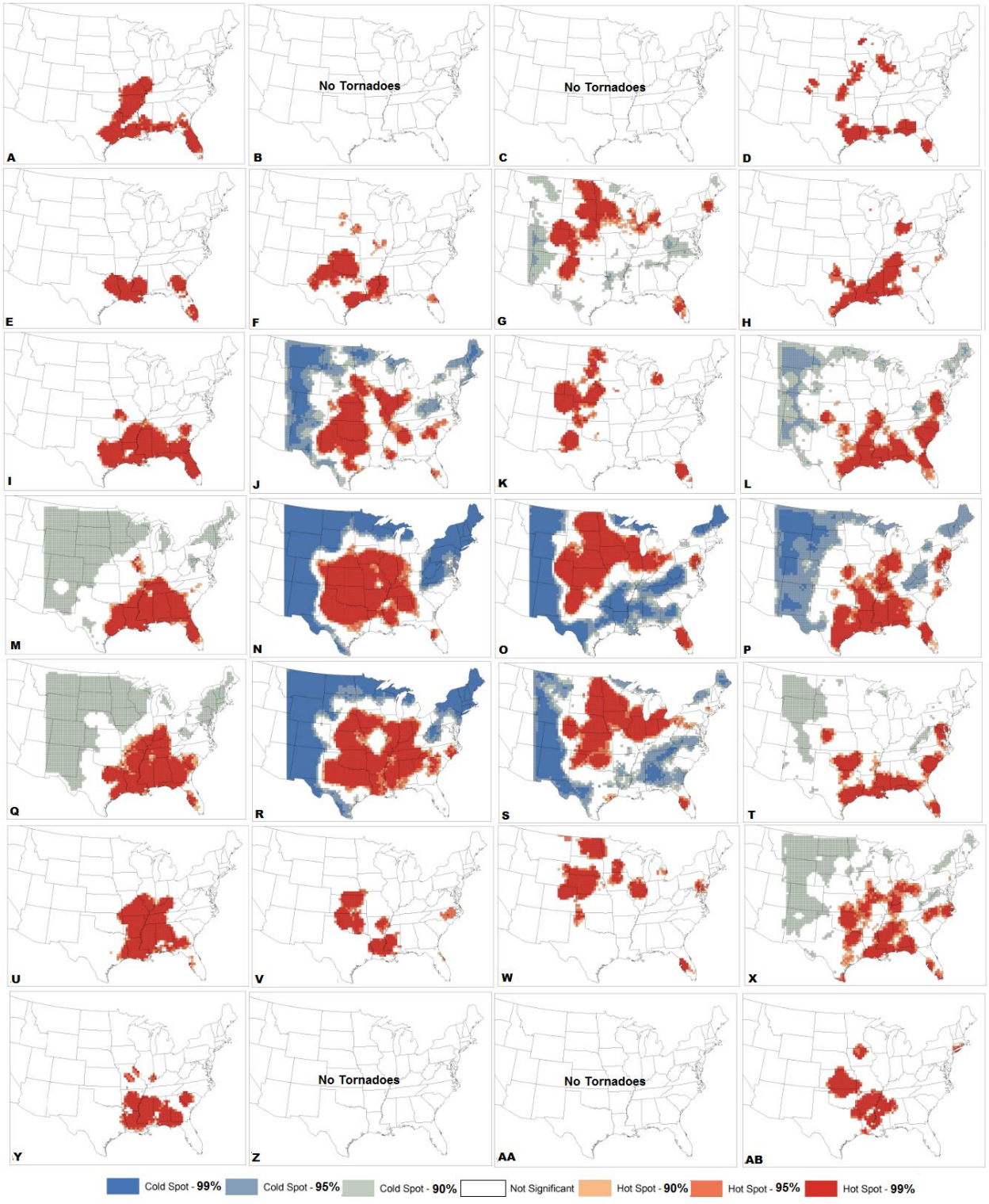

Figure 3.7: All tornado hot and cold spots, 1950-2014. Columns are in the order of winter, spring, summer and fall. A-D are Strong El Niño, E through H are Moderate El Niño, I through L are Weak El Niño, M through P are Neutral, Q through T are Weak La Niña, U through X are Moderate La Niña, and Y through AB are Strong La Niña.

Changes in spatial distribution of severe thunderstorm activity are attributed to the position of the jet stream (Barnes and Newton 1986; Johns and Doswell 1992; Cook and Schaefer 2008). The jet stream is modified by phase and intensity of ENSO (Cook and Schaefer 2008; Allen et al. 2015), as well as changes in season (Frauenfeld and Davis 2003; NWS 2016). Understanding the location of the jet stream is important because synoptic scale disturbances tend to form in areas of maximum wind speed and follow jet axes (Holton 1992), which modulates the location and intensity of severe weather (Archer and Caldeira 2008) and potentially tornado activity. The circumpolar vortex, which is a complex upper-level low-pressure area over the North Pole, is defined by geopotential contours that lie within the core of tropospheric westerlies (Frauenfeld and Davis 2003). Expansion (contraction) of the circumpolar vortex results in equatorward (poleward) modulation of the jet stream. Seasonal atmospheric analyses show that the largest shift in the jet stream and geopotential heights in the Northern Hemisphere was during summer in the circumpolar vortex (Frauenfeld and Davis 2003). The average latitude of the jet stream begins to shift poleward during spring and especially during summer with the contraction of the circumpolar vortex, then retreats towards the Equator in fall (NWS 2016). However, the intensity of the jet stream is strongest during winter, since the jet stream follows gradients between warm and cold air, which is most pronounced during winter (NWS 2016). Spatial evolution of hot spots in Figures 3.5 and 3.6 generally reflect the seasonal evolution of the circumpolar vortex and attendant jet stream, similar to Figure 3.7.

Strong spatial clustering is evident in the SEN plots across the southern U.S. for EF01 tornadoes (Figures 3.5A and 3.5D), like the all tornado pattern (Figure 3.7A and 3.7D). EF01 and EF25 tornado hot spots during SEN strongly resemble all tornado hot spots during the same phase. Fall SEN patterns show a striking difference between all (Figure 3.7D), EF01 (Figure

3.5D), and EF25 (Figure 3.6D) tornadoes. EF01 tornadoes show an increase in hot spot area along the Gulf, particularly in Florida, while EF25 tornadoes have a much smaller presence along the Gulf (Figure 3.6D). Therefore, we can say that EF01 tornadoes in the fall during a SEN typically to occur along the Gulf coast, while EF25 tornadoes are less likely in this region. Verification of this pattern can be done with gridded tornado counts, which is a point of future research beyond this study.

In MEN, hot spots of all tornadoes (Figure 3.7E) and EF01 tornadoes (Figure 3.5E) are almost identical in all four seasons. Unfortunately, only 28 strong tornadoes occurred in MEN winters, which was an insufficient sample size for the hot spot analysis. Hot spots amongst the other three seasons strongly resembled the distribution of hot spots of all tornadoes (Figure 3.7). Overall, fall MEN tornadoes do not show much variation from all tornadoes between EF01 and EF25 tornado hot spot location.

WEN tornadoes in winter show a persistent hot spot over the Gulf Plains regardless of tornado intensity, however there is a hot spot over most of Georgia and South Carolina for EF01 tornadoes (Figure 3.5I) that is not found for EF25 tornadoes (Figure 3.6I). In spring WEN, hot spots are similar for EF01 and EF25 tornadoes. WEN tornadoes in summer show an additional cold spot with the EF01 tornado analysis (Figure 3.5K), different from the all tornado analysis (Figure 3.7K). It is hypothesized that for the all tornado analysis, enough EF25 tornadoes exist along the cold spot region visible in Figure 3.5K to discount a significant cold spot, but not enough to result in a significant hot spot which is not visible in Figure 3.7K. The massive hot spot over Florida for EF01 tornadoes, and not EF25 tornadoes, could be the result of tornadoes spawning from hurricanes. In fall, EF01 tornadoes have significant hot spots along the entire Gulf Coast, while EF25 tornadoes solely lie near the Louisiana/Mississippi region.

Neutral tornadoes in winter do not show much variation between EF01 and EF25, with the exception of a strong tornado hot spot over northwest Illinois not present in EF01 tornadoes (Figure 3.6M). In fact, there is a lack of variation between all, EF01, and EF25 tornadoes for all four seasons during this phase. The only difference between tornado intensities occurs during summer, where tornado hot spots over Oklahoma and the Texas panhandle exist only for EF01 tornadoes, and disappear for EF25 tornadoes (Figure 3.5O and 3.6O).

For the WLN phase in winter, hot spots are unique to South Carolina and east Texas only for EF01 tornadoes, but not EF25 tornadoes (Figure 3.5Q). In spring, there seems to be a slight rotation in tornado hot spots between weak and strong tornadoes. EF01 tornadoes in spring have a much larger presence over the central U.S., specifically north Texas through Nebraska, while EF25 tornadoes show a shift primarily over the northern Dixie Alley (Figures 3.5R and 3.6R). EF25 tornadoes in summer during this phase show a unique presence over Oklahoma (Figure 3.6S) that is not evident in EF01 tornadoes (Figure 3.5S). In fall, EF01 tornadoes are likely to occur across the entire Gulf coast region, as well as Oklahoma and northeast Virginia (Figure 3.5T), whereas EF25 tornadoes are not likely (Figure 3.6T).

MLN tornadoes in winter show a northerly shift in hot spots away from the GOM for EF25 tornadoes when compared to EF01 ones. Spring tornadoes during this phase show an interesting area of hot spots for EF25 tornadoes in Arkansas (Figure 3.6V) that is not present for EF01 tornadoes (Figure 3.5V). Summer EF25 tornadoes during a MLN result in very little hot spots – this could be due to a smaller sample size. However, fall shows a similar pattern to winter; EF01 tornadoes are more likely to occur along the coastline (Figure 3.5X), while EF25 tornadoes exist more inland (Figure 3.6X).

Finally, winter tornadoes during a SLN are more likely to be classified as EF01 tornadoes

over Arkansas and Missouri, and rated EF25 over South Carolina (Figures 3.5Y and 3.6Y). The fall shows an interesting change in hot spot patterns when comparing EF25 tornadoes (Figure 3.6AB) to all tornadoes (Figure 3.7AB). Both EF01 and all tornadoes exhibit hot spots over the central plains, primarily over Arkansas and the Oklahoma/Kansas border. However, this area size increases drastically when examining only EF25 tornadoes. This is indicative that spatially, EF25 tornadoes (potentially from tornado outbreaks) are responsible for many of the hot spot locations.

Overall, the location of tornado hot spots dependent on tornado intensity does not vary greatly tornado hot spots of the entire dataset. There are small differences between a few select ENSO phases, which will be discussed in section 3.4, but those differences are most likely due to mesoscale processes and are therefore outside the scope of this research.

3.3.3 Adjusted Tornado Counts

To eliminate the upward trend in tornado counts over time, due to factors such as urbanization, population increase, and improvement in radar technology (Brooks et al. 2003; Lee et al. 2016), the Storm Prediction Center developed a simple method to eliminate this issue using a linear regression equation (Brooks and Carbin 2007). An analysis on raw tornado counts during varying phases of ENSO might be questioned due to the obvious upward trend in reports since 1950, necessitating this detrended analysis. While this method can remove the trend in tornado reports due to changes in detection and reporting, it cannot remove the potential influence of other external variables such as climate change and additional teleconnections. Figure 3.8 is an example of one of these calculations, which compares the raw values (Figure 3.8A) and adjusted values (Figure 3.8B).

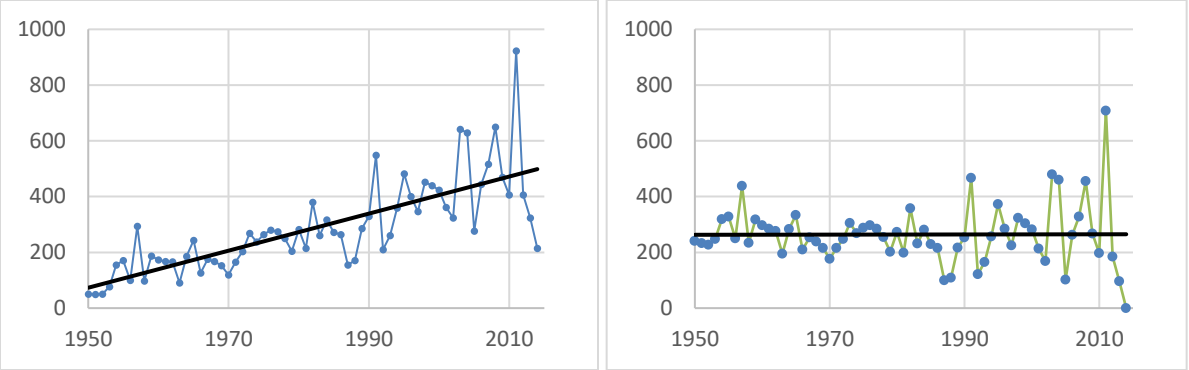

Figure 3.8: Raw (A) and adjusted (B) tornado counts for weak tornadoes in spring, 1950-2014

Annual tornado frequency is first plotted from 1950-2014. This upward tick in tornado counts is easily visible with a linear trend line, shown in black. The linear trend line equation is used to compute the "delta", which is the linear equation value for that year minus the original annual total, which results in the adjusted tornado count for that year (Brooks and Carbin 2007). For raw tornado counts for weak tornadoes in spring (Figure 3.8A), the median was 264. Each individual delta (positive if the original value is above the trend line, negative if below) was applied to 264. The resulting value is the adjusted tornado count for that year. Adjusted tornado counts were calculated for all four seasons and both tornado intensities. Once an adjusted tornado count has been calculated for each year and each season, counts can be binned into their appropriate ENSO category per year. The total sum of each ENSO category was calculated, then normalized (or averaged) by the number of entries in that category. The purpose of this is to eliminate the influence of heavily represented categories in respect to lesser represented categories (i.e. neutral categories versus stronger categories). The results are in Figure 3.9. Adjusted tornado counts for all tornadoes are included for comparison (Figure 3.10). The average values were then used for statistical tests examining the difference of means, such as the Kruskal-Wallis and Mann-Whitney test.

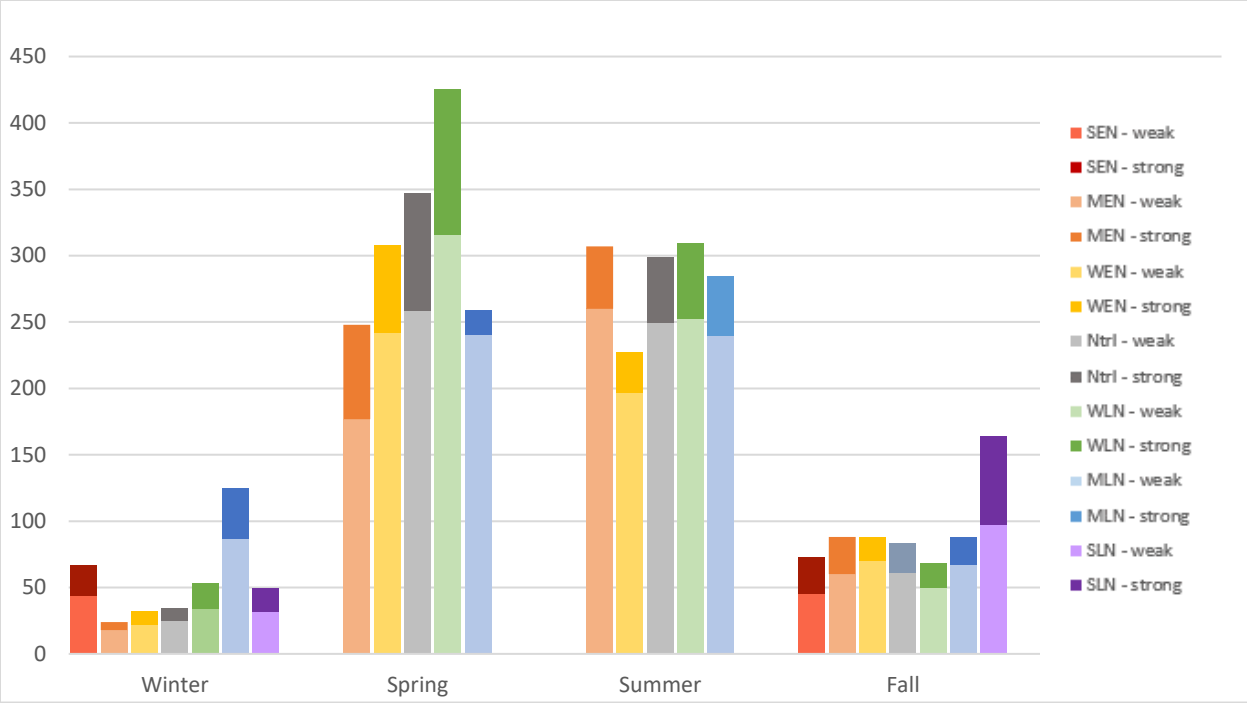

Figure 3.9: Detrended tornado counts per season across all phases of ENSO for both weak (light colors) and strong (dark colors) tornadoes, 1950-2014.

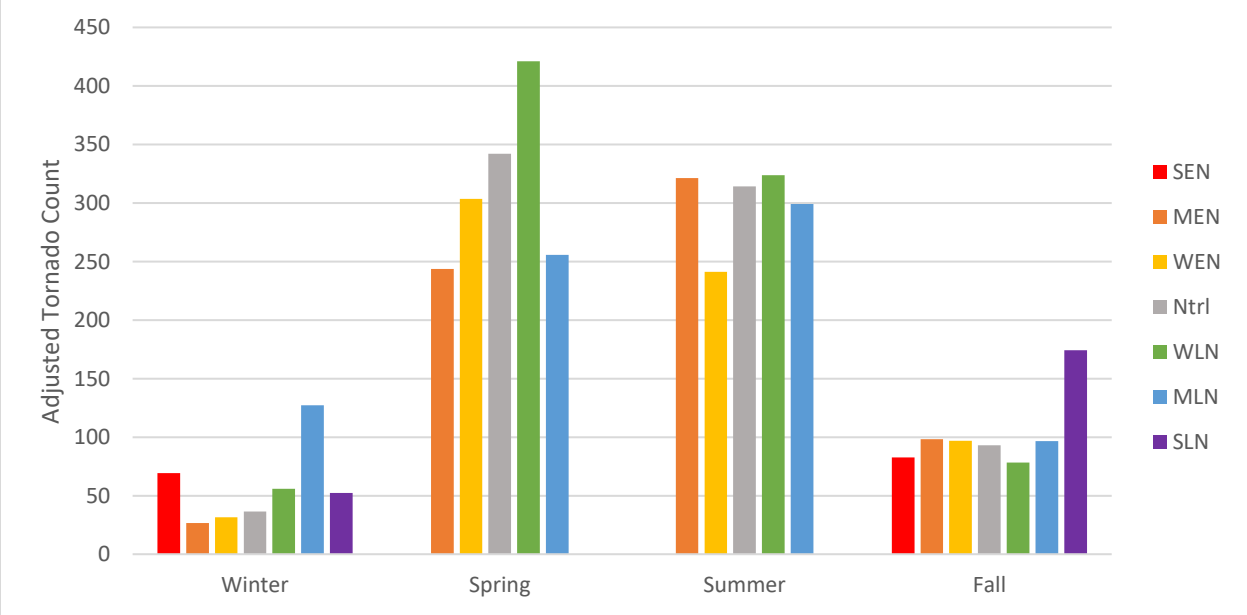

Figure 3.10: Detrended tornado counts for all tornadoes (for comparison), 1950-2014

To determine the appropriate statistics test, the data was tested for normality using both the Shapiro-Wilk test and Normal Quantile-Quantile (Q-Q) plots in R. When testing for normality, Q-Q plots are used to compare a sample distribution (i.e. adjusted tornado counts)

with a theoretical sample (i.e. a normal distribution, with a mean of zero and a standard deviation of one) (Vries and Meys 2015). The Shapiro-Wilk test was used secondarily to confirm findings from the Q-Q plots. The null hypothesis for the Shapiro-Wilk test is that the sample comes from a population which has a normal distribution (Royston 1982). Significant p-values would reject the null hypothesis, indicating that the sample has non-normal properties. Results for weak and strong tornadoes, with their respective Shapiro-Wilk p-values, are shown in Figures 3.11 and 3.12, respectively.

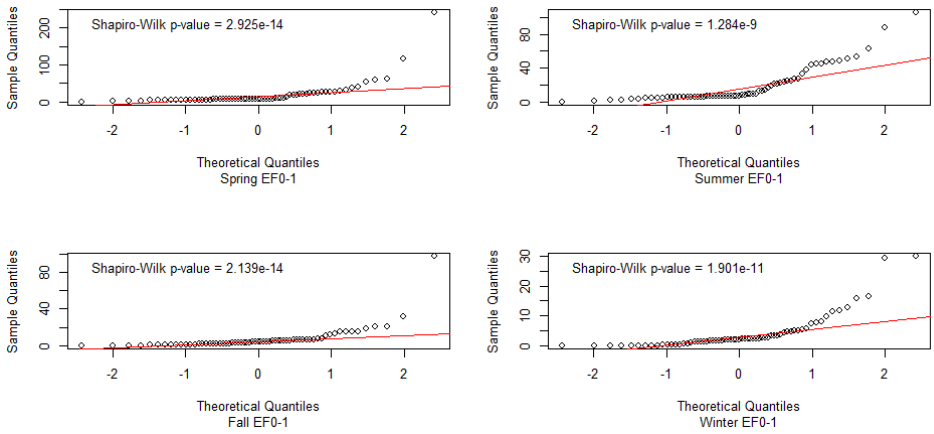

Figure 3.11. Seasonal normal Q-Q plots with Shapiro-Wilk p-value for weak tornadoes

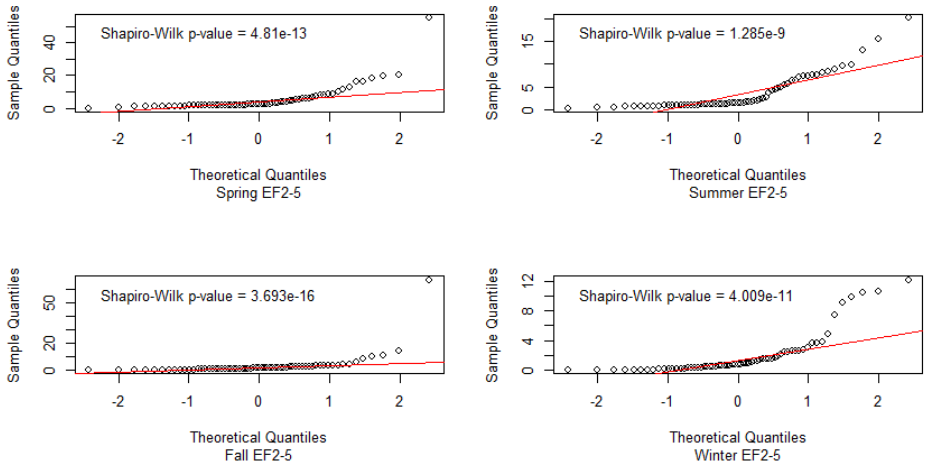

Figure 3.12. Seasonal normal Q-Q plots with Shapiro-Wilk p-value for strong tornadoes

With statistically significant p-values of less than .01 rejecting the null hypothesis of normality, as well as different observed and theoretical (in red) distributions from the Q-Q plots, the distribution of all data is confirmed to be non-normal, hence we will use non-parametric statistical tests on these data. As such, we test the differences between ENSO phases using the Kruskal-Wallis test, which is most appropriate because these data are unpaired (Kruskal & Wallis 1952; McKight and Najab 2010). The null hypothesis of the Kruskal-Wallis test is that there are no statistical differences between two or more groups of an independent variable (Aerd 2016). Results of the Kruskal-Wallis test for EF01 and EF25 tornadoes are in Table 3.1.

Table 3.1. Kruskal Wallis p-values for adjusted annual tornado counts

Season	Weak Tornadoes	Strong Tornadoes
Winter	< 0.001	< 0.001
Spring	< 0.001	< 0.001
Summer	< 0.001	< 0.001
Fall	< 0.001	< 0.001

Significant p-values reject the null hypothesis that there are no differences between two or more groups – in this case, "groups" are different phases of ENSO during each season. Therefore, these p-values indicate that at least one ENSO phase is different from the others for both EF01 and EF25 tornadoes. To specify exactly which ENSO phases are different from each other, the Mann-Whitney test was used. This test was used over the Wilcoxon because the pairs were unmatched, and the Wilcoxon test requires matched data ("Kruskal-Wallis and Friedman Tests" 2016). The Mann-Whitney U test is a simplified Kruskal-Wallis test, analyzing only two groups instead of multiple (McKight and Najab 2010). The Kruskal-Wallis was run first to determine if a Mann-Whitney should be applied to individual group (i.e. phase of ENSO), then the Mann-

Whitney was performed between each phase of ENSO. The Mann-Whitney is a measure of difference within mathematical space, or the difference in the location of the distribution.

Looking first at seasons, the increase in tornado counts across ENSO phases during spring is apparent through WLN for both EF01 and EF25 tornadoes. As ENSO transitions from MEN to WLN, the number of tornadoes increases from about 175 to over 300 in weak tornadoes, and about 60 to over 100 in strong tornadoes. The statistical difference between the five ENSO phases in spring are shown in Table 3.2 for EF01 tornadoes and Table 3.3 for EF25 tornadoes.

Table 3.2: Mann-Whitney resulting p-values for weak tornadoes in spring (very strong evidence – pink; strong – orange; moderate – yellow; weak or none – dark grey; no data – light gray)

	Strong El Niño	Moderate El Niño	Weak El Niño	Neutral	Weak La Niña	Moderate La Niña	Strong La Niña
Strong El Niño							
Moderate El Niño		-	-	-	-	-	
Weak El Niño		0.0444	-	-	-	-	
Neutral		0.0021	< 0.001	-	-	-	
Weak La Niña		0.0220	0.2380	< 0.001	-	-	
Moderate La Niña		0.6667	0.2222	0.0465	0.1538	-	
Strong La Niña							

Table 3.3: Mann-Whitney resulting p-values for strong tornadoes in spring (very strong evidence – pink; strong – orange; moderate – yellow; weak or none – dark grey; no data – light gray)

	Strong El Niño	Moderate El Niño	Weak El Niño	Neutral	Weak La Niña	Moderate La Niña	Strong La Niña
Strong El Niño							
Moderate El Niño		-	-	-	-	-	
Weak El Niño		0.0889	-	-	-	-	
Neutral		0.0021	< 0.001	-	-	-	
Weak La Niña		0.0879	0.4269	5.8310E-12	-	-	
Moderate La Niña		1.0000	0.4444	0.0465	0.3077	-	
Strong La Niña							

Twelve out of the 20 relationships show statistical differences in the weak and strong category, consistent with all tornadoes. MLN returns mostly non-significant p-values for both, and this is likely due to the category only having one value, shown in the following box and whisker plots (Figures 3.13 and 3.14), resulting in non-significance. Therefore, it is important to

note that spring MLN frequencies should not be trusted as much as other tornado frequencies in spring.

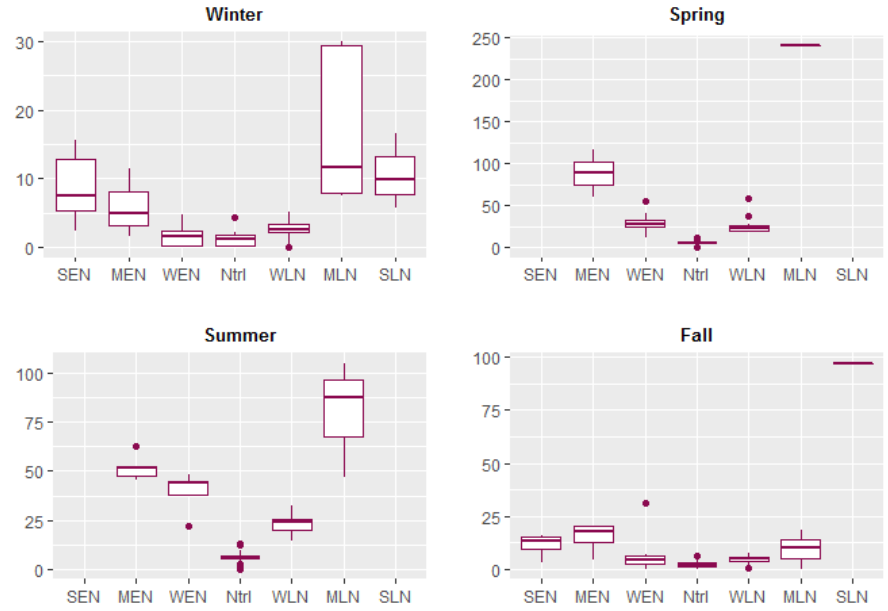

Figure 3.13: Box-and-whisker plots of weak tornado counts per season by ENSO phase

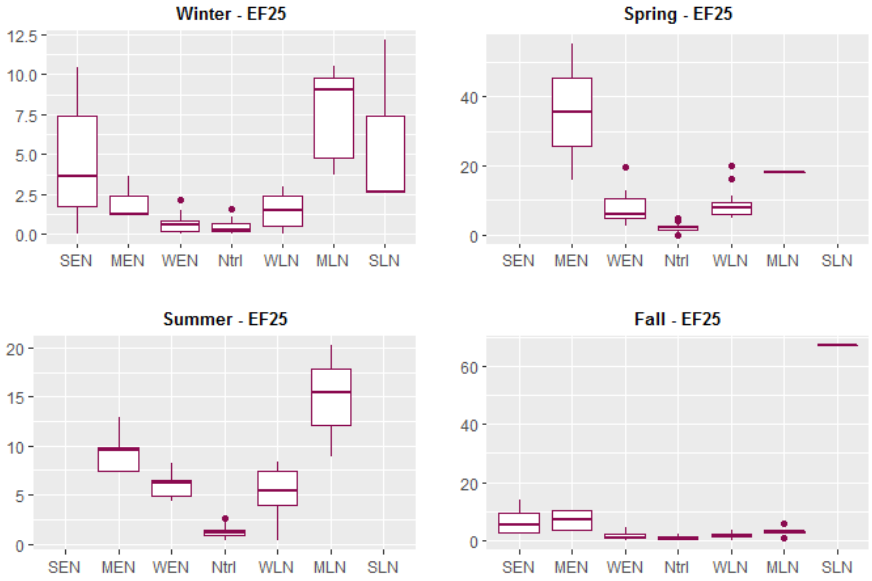

Figure 3.14: Box-and-whisker plots of strong tornado counts per season by ENSO phase

Summer shows distributions across ENSO phases that are relatively similar regardless of tornado intensity. This pattern is like the all tornadoes distribution (Figure 3.10), where it is even across all phases except for a decrease during WEN's. However, statistical tests show that the relationships between ENSO phases for both EF01 and EF25 tornadoes result in 17 out of 20 significantly different distributions (Tables 3.4 and 3.5).

Table 3.4: Mann-Whitney resulting p-values for weak tornadoes in summer (very strong evidence – pink; strong – orange; moderate – yellow; weak or none – dark grey; no data – light gray)

	Strong El Niño	Moderate El Niño	Weak El Niño	Neutral	Weak La Niña	Moderate La Niña	Strong La Niña
Strong El Niño							
Moderate El Niño		-	-	-	-	-	
Weak El Niño		0.0318	-	-	-	-	
Neutral		< 0.001	< 0.001	-	-	-	
Weak La Niña		0.0005	0.0133	< 0.001	-	-	
Moderate La Niña		0.3929	0.0714	0.0002	0.0055	-	
Strong La Niña							

Table 3.5: Mann-Whitney resulting p-values for strong tornadoes in summer (very strong evidence – pink; strong – orange; moderate – yellow; weak or none – dark grey; no data – light gray)

	Strong El Niño	Moderate El Niño	Weak El Niño	Neutral	Weak La Niña	Moderate La Niña	Strong La Niña
Strong El Niño							
Moderate El Niño		-	-	-	-	-	
Weak El Niño		0.0318	-	-	-	-	
Neutral		< 0.001	< 0.001	-	-	-	
Weak La Niña		0.0133	0.5833	6.1070E-06	-	-	
Moderate La Niña		0.2500	0.0357	0.0002	0.0055	-	
Strong La Niña							

Like the all tornadoes results (Figure 3.10), the adjusted counts drastically decrease when transitioning into fall and winter seasons. This is true for both EF01 and EF25 tornadoes. In fall, SLN has the largest counts in both EF01 and EF25 tornadoes, but the difference across ENSO phases is much more dramatic in EF25 tornadoes. The rest of the counts fall around the same value upon examination of EF25 tornadoes, but in EF01 tornadoes there is a secondary

peak during WEN. This is possibly due to an outlier in the distribution, shown in Figure 3.13. Tables 3.6 and 3.7 show that only 19 out of 42 relationships have statistically different distributions.

Table 3.6: Mann-Whitney resulting p-values for weak tornadoes in fall (very strong evidence – pink; strong – orange; moderate – yellow; weak or none – dark grey; no data – light gray)

	Strong El Niño	Moderate El Niño	Weak El Niño	Neutral	Weak La Niña	Moderate La Niña	Strong La Niña
Strong El Niño	-	-	-	-	-	-	-
Moderate El Niño	0.3429	-	-	-	-	-	-
Weak El Niño	0.1014	0.0785	-	-	-	-	-
Neutral	0.0013	< 0.001	0.0616	-	-	-	-
Weak La Niña	0.1040	0.0557	0.6443	0.0105	-	-	-
Moderate La Niña	0.7879	0.2303	0.1173	0.0082	0.1259	-	-
Strong La Niña	0.4000	0.4000	0.1410	0.0741	0.1667	0.2500	-

Table 3.7: Mann-Whitney resulting p-values for strong tornadoes in fall (very strong evidence – pink; strong – orange; moderate – yellow; weak or none – dark grey; no data – light gray)

	Strong El Niño	Moderate El Niño	Weak El Niño	Neutral	Weak La Niña	Moderate La Niña	Strong La Niña
Strong El Niño	-	-	-	-	-	-	-
Moderate El Niño	0.6857	-	-	-	-	-	-
Weak El Niño	0.0132	0.0044	-	-	-	-	-
Neutral	< 0.001	< 0.001	0.1744	-	-	-	-
Weak La Niña	0.0103	0.0015	0.4491	0.0139	-	-	-
Moderate La Niña	0.5273	0.0242	0.0221	0.0002	0.0441	-	-
Strong La Niña	0.4000	0.4000	0.1538	0.0741	0.1667	0.2500	-

Although fall SLN clearly has the highest adjusted count in both categories, statistically significant p-values only surface when compared to the Neutral phase. This is most likely due to a distribution of only one value; therefore, the frequency of tornado counts during fall SLN should not be trusted as much as the other six phases during fall. Winter shows a "U" shape across ENSO phases, with a large spike during MLN in both EF01 and EF25 tornadoes. In EF01 tornadoes, SEN has a relatively large tornado count, which decreases in the transition to MEN, and increases through the spectrum up through MLN. EF25 tornadoes show this same variation;

however, the actual tornado counts are so small that the variation itself is only over the span of 10 or so tornadoes amongst ENSO phases. A total of 26 out of 42 winter relationships are statistically different from each other (Tables 3.8 and 3.9).

Table 3.8: Mann-Whitney resulting p-values for weak tornadoes in winter (very strong evidence – pink; strong – orange; moderate – yellow; weak or none – dark grey; no data – light gray)

	Strong El Niño	Moderate El Niño	Weak El Niño	Neutral	Weak La Niña	Moderate La Niña	Strong La Niña
Strong El Niño	-	-	-	-	-	-	-
Moderate El Niño	0.3929	-	-	-	-	-	-
Weak El Niño	0.0039	0.0965	-	-	-	-	-
Neutral	0.0009	0.0358	0.5406	-	-	-	-
Weak La Niña	0.0140	0.3643	0.0253	0.0016	-	-	-
Moderate La Niña	0.2222	0.1429	0.0012	0.0007	0.0002	-	-
Strong La Niña	0.5714	0.4000	0.0090	0.0067	0.0036	0.5714	-

Table 3.9: Mann-Whitney resulting p-values for strong tornadoes in winter (very strong evidence – pink; strong – orange; moderate – yellow; weak or none – dark grey; no data – light gray)

	Strong El Niño	Moderate El Niño	Weak El Niño	Neutral	Weak La Niña	Moderate La Niña	Strong La Niña
Strong El Niño	-	-	-	-	-	-	-
Moderate El Niño	0.3929	-	-	-	-	-	-
Weak El Niño	0.0359	0.0575	-	-	-	-	-
Neutral	0.0234	0.0040	0.4315	-	-	-	-
Weak La Niña	0.1433	0.7036	0.0448	< 0.001	-	-	-
Moderate La Niña	0.2222	0.0357	0.0012	< 0.001	< 0.001	-	-
Strong La Niña	0.7857	0.4000	0.0090	< 0.001	0.0393	0.5714	-

Overall, 75 out of 124 relationships when comparing weak and strong tornadoes across varying ENSO phases seasonally are statistically different from each other (about 60%).

To compare EF01 and EF25 tornadoes against the entire record, ENSO phases were compared against their own phase in another category. For example, SEN in spring for EF01 tornadoes was compared against SEN in spring for all tornadoes. The resulting table is shown below (Table 3.10).

Table 3.10: Seasonal Mann-Whitney resulting p-values when comparing all vs. weak, all vs. strong, and weak vs. strong tornadoes

		Strong El Niño	Moderate El Niño	Weak El Niño	Neutral	Weak La Niña	Moderate La Niña	Strong La Niña
Spring	All vs. Weak	-	0.6670	0.3282	< 0.001	0.0121	1.0000	-
	All vs. Strong	-	0.3333	0.0003	< 0.001	< 0.001	1.0000	-
	Weak vs. Strong	-	0.3333	0.0006	< 0.001	< 0.001	1.0000	-
Summer	All vs. Weak	-	0.0556	0.1508	< 0.001	0.0192	0.4000	-
	All vs. Strong	-	0.0079	0.0079	< 0.001	2.8350E-06	0.1000	-
	Weak vs. Strong	-	0.0079	0.0079	< 0.001	2.8350E-06	0.1000	-
Fall	All vs. Weak	0.2000	0.2000	0.2141	0.0256	0.0083	0.3176	1.0000
	All vs. Strong	0.0571	0.1143	0.0011	< 0.001	< 0.001	0.0175	1.0000
	Weak vs. Strong	0.2000	0.1143	0.0262	< 0.001	0.0019	0.0379	1.0000
Winter	All vs. Weak	0.4206	0.7000	0.2206	0.1180	0.0428	0.2222	0.7000
	All vs. Strong	0.0952	0.1000	0.0151	0.0016	0.0013	0.0079	0.2000
	Weak vs. Strong	0.2222	0.2000	0.1508	0.0345	0.0612	0.2222	0.4000

When comparing EF01 tornadoes versus all tornadoes, 2 out of 5 were significant in spring, 3 out of 5 were significant in summer, 2 out of 7 were significant in fall, and 1 out of 7 in winter. The lack of significantly different results is not surprising, considering the distribution of tornado counts is not all that different between the EF01 tornado dataset and all tornado dataset (Figures 3.9 and 3.10). All tornadoes versus EF25 tornadoes resulted in 3 out of 5 significant differences in spring, 5 out of 5 in summer, 5 out of 7 in fall, and 6 out of 7 in winter. In other words, 19 out of 24 inter-relationships when examining all tornadoes vs. EF25 tornadoes were statistically different from each other. Finally, by comparing EF01 tornadoes versus EF25 tornadoes, it was found that 3 out of 5 were significant in spring, 5 out of 5 were significant in summer, 4 out of 7 were significant in fall and 3 out of 7 were significant in winter.

In summary, based on adjusted count analysis alone, only 33% of phases were statistically different between EF01 tornadoes and all tornadoes, 80% of phases showed significantly different values between EF25 and all tornadoes, and 63% were significant when comparing EF01 against EF25. Between EF01 and EF25 tornadoes, summer showed the most

significant differences between ENSO phases with all five relationships resulting in significant p-values. Spring follows, with three out of five. The distribution of tornadoes for the entire record versus the EF01 record is quite similar, resulting in little difference between the two. This is visible in Figures 3.9 and 3.10. In short, ENSO seems to have a significant influence on the number of tornadoes, but the overall distribution does not vary when broken down by tornado intensity.

3.3.4 Tornado Days and the Destruction Potential Index

The Destruction Potential Index (DPI) is an index of the total tornado damage area for each day (in this study, a "tornado day") multiplied by the weighted mean F-scale for all tornadoes within that time period (Thompson and Vescio 1998). It is a measure of the potential for damage and causalities within a particular outbreak. The DPI is used here to examine the influence that ENSO has on tornado days during specified phases and seasons, as well as further understand the influence ENSO has on tornado strength and path area. The DPI formula is described in Equation 3.1. Tornado days are defined as a day that has 6 or more tornadoes occurring within a 24-hour period, to be consistent with Cook and Schaefer (2008) and Galway (1975). After each ENSO-tornado dataset was stratified into records falling on a tornado day, the DPI was calculated for each tornado day. The total number of tornado days, average tornado days per season, total DPI for all tornado days and average DPI per for all tornado days are shown in Table 3.11. Average DPI across all seasons are displayed in Figure 3.15.

Table 3.11: Tornado day and resulting DPI values across all seasons and phases of ENSO

Spring									
	SEN	**MEN**	**WEN**	**Ntrl**	**WLN**	**MLN**	**SLN**	**Sum**	**χ^2 statistic**
Total number of "tornado days"	-	31.0	116.0	842.0	274.0	4.0	-	1267.0	31.71
Average number of "tornado days" per spring	-	15.5	14.5	20.0	22.8	4.0	-	76.9	155.74
Number of springs according to ENSO phase	-	2.0	8.0	42.0	12.0	1.0	-	65.0	-
Total DPI for all "tornado days"	-	468.0	4781.6	39745.8	23784.4	66.1	-	68845.9	13979.37
Average DPI for all "tornado days"	-	15.1	41.2	47.2	86.8	16.5	-	206.8	3680.46
Summer									
Total number of "tornado days"	-	92.0	65.0	736.0	179.0	53.0	-	1125.0	7.39
Average number of "tornado days" per summer	-	18.4	13.0	18.0	16.3	17.7	-	83.3	189.23
Number of summers according to ENSO phase	-	5.0	5.0	41.0	11.0	3.0	-	65.0	-
Total DPI for all "tornado days"	-	663.3	620.2	8922.4	2545.6	348.1	-	13099.5	476.91
Average DPI for all "tornado days"	-	7.2	9.5	12.1	14.2	6.6	-	49.7	35.37
Fall									
Total number of "tornado days"	20.0	16.0	48.0	128.0	46.0	42.0	9.0	309.0	8.96
Average number of "tornado days" per fall	5.0	4.0	4.0	4.9	4.2	6.0	9.0	37.1	96.90
Number of falls according to ENSO phase	4.0	4.0	12.0	26.0	11.0	7.0	1.0	65.0	-
Total DPI for all "tornado days"	376.1	972.8	1191.2	4401.6	553.9	694.2	151.0	8340.8	1438.65
Average DPI for all "tornado days"	18.8	60.8	24.8	34.4	12.0	16.5	16.8	184.2	3743.23
Winter									
Total number of "tornado days"	21.0	9.0	35.0	52.0	41.0	36.0	15.0	209.0	36.43
Average number of "tornado days" per winter	4.2	3.0	2.3	2.5	3.2	7.2	5.0	27.4	110.64
Number of winters according to ENSO phase	5.0	3.0	15.0	21.0	13.0	5.0	3.0	65.0	-
Total DPI for all "tornado days"	507.5	81.8	659.2	1477.2	1505.3	2548.1	217.9	6997.1	8566.14
Average DPI for all "tornado days"	24.2	9.1	18.8	28.4	36.7	70.8	14.5	202.5	3923.27

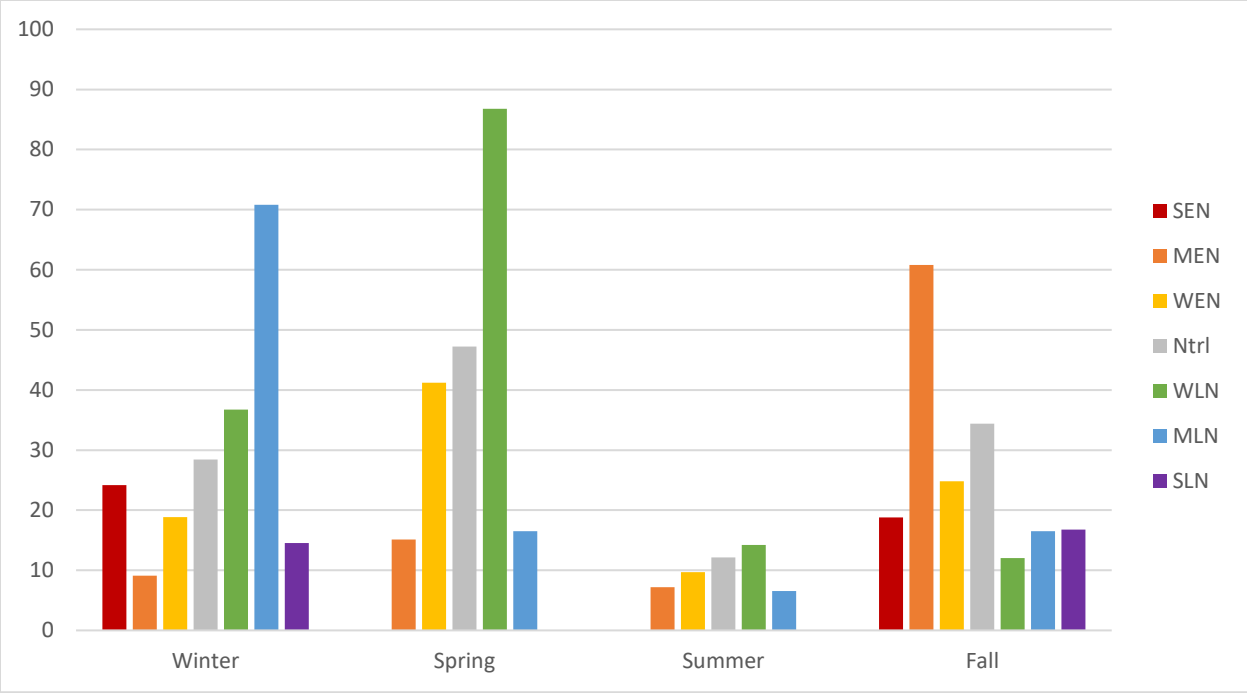

Figure 3.15: Average DPI results across all seasons and phases of ENSO

A χ^2 distribution is used to determine whether the distribution of these parameters varies with ENSO phase. If the χ^2 statistic is larger than the critical value, the hypothesis that the distributions are independent of the respective ENSO phase can be rejected. The formula to calculate this statistic is described in Equation 3.2.

$$\chi^2 = \sum \frac{(\text{\# Observed - \# Expected})^2}{\text{\# Expected}} \qquad \textbf{3.2}$$

For each metric (i.e. tornado days, DPI, etc.), the expected value was calculated as the sum of that metric times the number of seasons in respective ENSO phase, divided by the total number of seasons on record (in this study, the total number of seasons is 65). For example, in spring MEN, the expected value for total DPI for all tornado days was calculated by multiplying the total DPI observed across all ENSO phases in spring by the number of seasons in spring MEN (2), divided by 65. Doing this across all ENSO phases, and summing the totals results in the chi-

square statistic. The critical value (v) is determined by subtracting one from the number of classes. In spring and summer, v is 4. For fall and winter, v is 6. The confidence levels for each critical value is from Wilks (1995). For a critical value equal to 4, the 90% confidence interval is 7.779 and the 99.9% confidence interval is 23.512. For the critical value 6, the 90% confidence interval is 10.645 and the 99.9% confidence interval is 27.855.

In Table 3.11, the χ^2 statistic for tornado days in spring and winter (31.71 and 36.43) are above the 99% critical level of 23.512 and 27.855, respectively. Summer and fall show less significant χ^2 statistics of 7.39 and 8.96, respectively, which fall below even the 90% critical level of 7.779 and 10.645, respectively. Therefore, for summer and fall, we cannot reject the null hypothesis that the frequency of tornado days over the eastern U.S. is independent of ENSO phase. However, in winter and spring, because the χ^2 statistic is larger than the critical level at as high as the 99.9% confidence level, the hypothesis that the frequency of tornado days in the study area are independent of ENSO phase can be rejected. In other words, in spring and winter, the total number of tornado days east of the Rocky Mountains is affected by ENSO phase. The χ^2 test is also used to determine whether the DPI observations have statistical significance. The χ^2 statistic for ENSO-related differences in the average DPI for spring, summer, fall, and winter tornado days (3,680.46, 35.37, 3,743.23, and 3,923.27, respectively) is well above the 99.9% confidence level for all four seasons (23.512 for spring and summer, and 27.855 for fall and winter). Therefore, we can reject the hypothesis that average DPI for spring, summer, fall and winter tornado days is independent of ENSO phase.

Average DPI (Figure 3.15) shows considerable differences between ENSO phases across each season. In winter, DPI tends to be the highest during MLN. DPI decreases as ENSO transitions from La Niña to El Niño, apart from a spike during SEN. Spring WLN has the highest

DPI for its season, which again decreases in its transition from La Niña to El Niño. In fact, spring WLN has the highest DPI for all seasons. Historically, spring Weak La Niña has coincided with some of the most devastating tornado outbreaks in recorded history. In terms of DPI, the top five include dates such as April 27th, 2011 (207 tornadoes with a DPI of 6,236), April 3rd 1974 (128 tornadoes with a DPI of 2384), May 31st, 1985 (30 tornadoes with a DPI of 116), and May 24th, 2011 (48 tornadoes with a DPI of 1060). The presence of some of the largest outbreaks in history occurring during spring WLN is consistent with large hot spots (Figure 3.7) and increased tornado counts (Figures 3.10) shown in both analysis chapters. Summer shows the smallest variation in DPI values; however, it follows the same trend with WLN showing the largest DPI, and decreasing as La Niña turns into El Niño. Fall is the exception to the trend, with the largest DPI occurring during MEN then varying non-harmoniously across ENSO phases and intensities. Large DPI values indicate long-track, strong tornadoes. Therefore, in winter, spring and summer, La Niña phases are more favorable for long-track, strong tornadoes, with WLN being more favorable for these conditions in spring and summer, and a MLN in winter. In fall, a MEN phase is more favorable for longer, more intense tornadoes, with a non-uniform pattern in the remaining ENSO phases. It's noteworthy to mention the much smaller DPI values in summer when compared to the rest of the seasons. As a whole, spring and summer have the most tornadoes on record (Figure 3.10). Table 3.11 reveals that the number of tornado days and the average number of tornado days per season is much larger in summer than in fall and winter. Therefore, the large decrease in DPI during this season must be due to weak, short-lived tornadoes occurring in outbreaks.

3.4 Discussion

EF01 and EF25 tornadoes exhibited geographic dependence on seasonality and ENSO

phase, but did not differ from those patterns exhibited for all tornadoes (Figures 3.5, 3.6, and 3.7). Tornado frequencies for both weak and strong tornadoes strongly resembled the distribution of all tornadoes as well (Figures 3.9 and 3.10). However, three different phases of ENSO did show variation between EF01 and EF25 tornado hot spots, and those maps will be discussed here.

From a seasonal perspective, both Strong El Niño seasons (fall and winter) showed interesting variations between weak and strong tornado hot spots. In winter, most EF01 tornado hot spots are oriented along an east-west axis along the Gulf coast, extending from east Texas into Florida (Figure 3.16A), while EF25 tornado hotspots are oriented along a southwest-northeast axis from northeast Texas to southern Illinois (Figure 3.17B). The absence of strong tornadoes along the GOM could be due to weak tornadoes spawning from extratropical cyclones in the NW GOM, which have been shown more frequent during El Niño years (Hardy and Hsu 1997). This same observation could be made for weak tornadoes during fall SEN, where more weak tornadoes are oriented along the GOM (Figure 3.16C) and stronger tornadoes have smaller hot spots over Illinois and Indiana (Figure 3.16D) There are likely potential factors influencing the occurrence of weak tornadoes along the coastline (due to cyclogenesis in the GOM), and strong tornadoes further north in the U.S., which are outside the scope of this research and could benefit from future analysis. The geographical difference in hot spots is more minimal during a spring WLN (Figures 3.16E and 3.16F), but there are differences between the two. Weak tornadoes hot spots occur over Kansas and Nebraska, which does not show up for strong tornadoes. On the other hand, strong tornadoes exhibit a hot spot over Alabama/Georgia, which is not present for weak tornadoes.

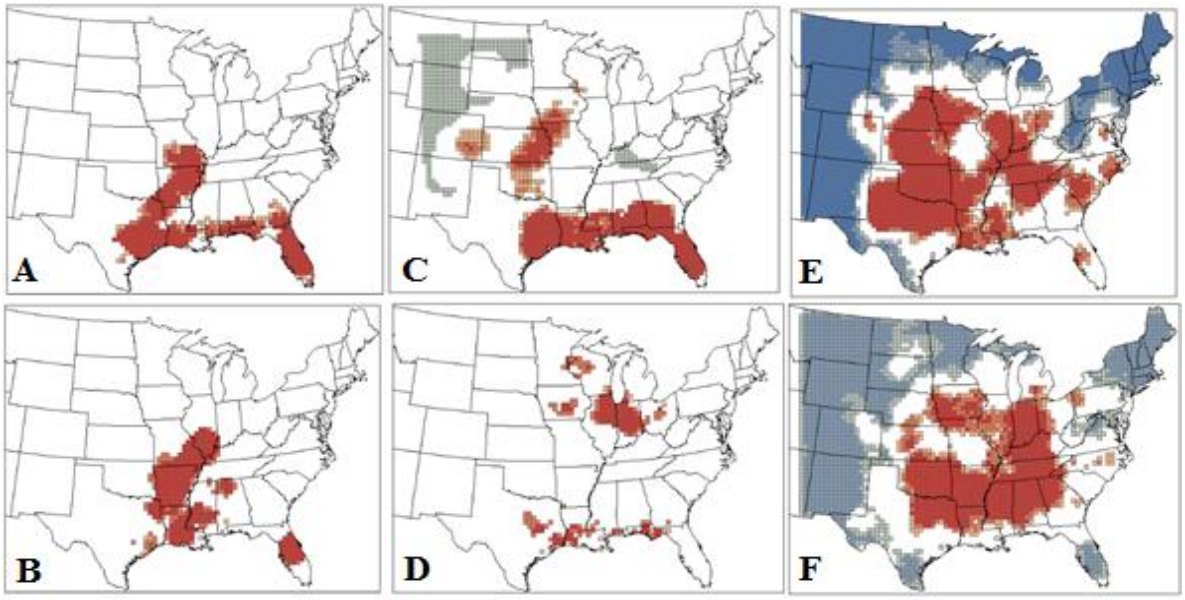

Figure 3.16: Comparisons of weak vs. strong tornadoes. Winter SEN weak (A) vs. strong (B), Fall SEN weak (C) vs. strong (D), and Spring WLN weak (E) vs. strong (F) tornadoes are shown.

Unfortunately, there is not a clear reason why changes in physical location between weak and strong tornadoes are occurring. The purpose of this research is to study the influence ENSO has on synoptic scale features impacting severe weather activity, and potentially tornado activity, in the eastern U.S. To assess changes in tornado intensity, synoptic scale patterns might not be enough. The location of one hot spot for weak tornadoes that does show up for strong tornadoes could be due to something as simple as one outbreak. For example, the spring 2011 tornado outbreaks across the southeastern U.S., which produced many strong tornadoes, could be the cause for hot spots over Alabama/Georgia that do not appear in weak tornadoes. To fully understand what is influencing a change in geographic location by tornado intensity, a mesoscale or daily atmospheric assessment is necessary to attempt to relate the influence of ENSO. Future research could take these factors into account to better analyze the role ENSO plays in tornado intensity location across the southeastern U.S.

3.5 Conclusion

Tornadoes from 1950 through 2014 were analyzed geographically as a function of ENSO to test the relationship against varying tornadic intensities, tornado days, and the Destruction Potential Index. A seasonal Niño 3.4 index was derived from the original Niño 3.4 index to better represent tornadic activity seasonally without involving a running 3-month mean (used in the ONI). Spatial statistics such as the average nearest neighbor distance and Global Moran's I were performed first on weak (EF-0 and EF-1) and strong (EF-2 through EF-5) tornadoes to confirm spatial clustering, then local statistics (Optimized Hot Spots) were applied to visualize where spatial clustering was occurring across the study region. Annual tornado counts were detrended to remove the upward trend observed in tornado counts due to urbanization, technology improvements and population increase. These adjusted tornado counts were analyzed as a function of ENSO for both weak and strong tornadoes to determine if ENSO influences tornadic intensity. To analyze whether ENSO influences the strength and length of tornadoes, the Destruction Potential Index was used. Tornado days were defined as a 24-hour period that had 6 or more tornadoes, and a DPI was calculated for each outbreak and averaged across an ENSO season to test its role. The chi-square statistic was implemented to test the significance of these findings. It was found that in general, the overall pattern of weak versus strong tornadoes does not vary from all tornadoes dependent on ENSO phase. In spring, a Weak La Niña means more tornadoes for both weak and strong tornadoes (Figure 3.9). The DPI was also significant during this season and phase (Figure 3.15); spring Weak La Niña had the largest average DPI out of any season and phase of ENSO. This means that stronger, longer-lived tornado tracks and outbreaks occur during Weak La Niña in the spring. The hot spots verify this claim, with the second-largest hot spot for strong tornadoes occurring (only behind spring Neutral). Summer has a relatively even distribution of tornado counts across ENSO phase, with Weak El Niño showing slightly

smaller annual frequency in both weak and strong tornadoes. Perhaps the most interesting result for this season is the extremely small DPI values with respect to other seasons. Though there is a slight increase in average DPI from El Niño to La Niña, the difference between them is quite small. A small DPI indicates weaker, shorter tornadoes. This is verified in the hot spot maps, where the strong tornado analysis reveals smaller significant tornado locations compared to other seasons (Figure 3.6, column 3). Fall has its largest tornado count during Strong La Niña for both weak and strong tornadoes. An examination of spatial hot spots does not reveal a specific geographic shift dependent on ENSO phase; however, the Moderate El Niño phase does have the largest average DPI, indicating strong and longer tornadoes, which is reflected by a stronger band of hot spots (Figure 3.6H). Winter also shows a slight lean toward higher tornado counts during La Niña phases for both weak and strong tornadoes, except for a Strong El Niño phase. As ENSO transitions from El Niño to La Niña, a general northward expansion of hot spots exists through Moderate La Niña. The average DPI suggests that Moderate La Niña is most conducive for longer and stronger tornadoes. Geographical variation between weak and strong tornadoes did not differ from the all tornado analysis, with shifts being attributed to seasonality and ENSO phase and not tornado intensity. Three hot spot maps showcasing differing hot spots by tornado intensity were shown, but verifying the reason atmospherically was outside the scope of this study. All average DPI values returned with a significant chi-square statistic, meaning that tornado days in all four seasons are dependent on ENSO phase. The statistical differences between adjusted tornado counts across ENSO phases for strong, weak, and all tornadoes were tested using the Mann-Whitney test. Only 33% of phases were statistically different between weak tornadoes and all tornadoes, 80% of phases showed significantly different values between strong and all tornadoes, and 63% were significant when comparing weak against strong. This

indicates that the weak tornado record and all tornado record distribution are roughly similar, the strong tornado record and all tornado record are largely different, and the distributions between weak and strong tornadoes are also different. Though the pattern of tornado frequencies across ENSO phases is not different compared to all tornadoes, the intensity of ENSO does seem to have an impact on tornado frequencies between weak and strong tornadoes. Overall, this study does conclude that ENSO has an influence on tornadoes in the eastern United States. Tornado frequencies generally tend to be higher during La Niña phases. A larger sample size would be beneficial to the moderate and strong phases of El Niño and La Niña; future studies could improve this type of study with a longer time period to resolve this issue. Future research could utilize the seasonal findings of this study through machine-based learning to create a functional prediction tool, which has been studied previously but only for spring (LaCorte 2011).

CHAPTER 4: SUMMARY AND CONCLUSION

Large tornado outbreaks coinciding with specific phases and intensities of ENSO, as well as conflicting results in the literature, have raised concerns that the teleconnection has an influence on tornadic activity in the eastern United States which we do not understand fully. For this reason, tornado frequency and spatial distribution in the eastern United States were examined as a function of ENSO to gain an understanding of the ENSO-tornado relationship. In addition, spatial and annual frequencies were examined for weak and strong tornadoes, and tornado days were analyzed to calculate a Destruction Potential Index to examine the influence ENSO has on tornado track area seasonally. The results of this study have implications on seasonal tornado outlooks, as this type of study has not been performed on summer and fall. The following summarizes the seminal results of this thesis, based on the objectives noted in Chapter 1.

4.1 Objective 1 – Tornado frequencies related to ENSO

Annual tornado frequencies were detrended to analyze the influence that ENSO has on tornado counts seasonally. This was done with the Storm Prediction Center linear regression method, to eliminate the natural increase in tornado observations due to urbanization, improvement in technology (i.e. Doppler radar), and increased eyewitness reports from population increases over time. It was found that spring and summer have the most tornado counts regardless of ENSO phase, and fall and winter have roughly similar counts. In spring, as ENSO transitions from Moderate El Niño to Weak La Niña, tornado counts increase. A strong El Niño phase means fewer tornadoes, and a Weak La Niña is most conducive for tornado activity. Results during a Moderate La Niña in spring should not be trusted due to small sample size and

non-significance via the Mann-Whitney test. Summer shows less variation in counts across ENSO phases, with the exception of a decrease in counts during Weak El Niño. Fall and winter both show larger annual frequency during La Niña phases; Strong La Niña in fall, and Moderate La Niña in winter. However, Strong La Niña results in fall should not be relied on due to a small sample size and non-significant Mann-Whitney results. These annual frequencies were tested for statistical significance using the Mann-Whitney test, and 40 out of 62 individual relationships between two groups resulted as statistically different (64.5%). The same analysis was performed on weak (EF-0 through EF-1) and strong (EF-2 through EF-5) tornadoes, and the distribution of tornado counts across ENSO phases was similar, just with smaller counts. When weak tornadoes were compared against the entire record, only 33% of phases were statistically different. Strong tornadoes resulted in 80% significantly different values when compared against the entire record, and 63% of were significant when comparing weak against strong. These results meet the first objective that tornadic frequency varies across ENSO phase for all, weak, and strong tornadoes.

4.2 Objective 2 – Geographical distribution of tornadoes by ENSO phase

Tornadoes were stratified by ENSO phases based on the seasonal Niño 3.4 index to examine geographical distribution across the eastern United States. This was accomplished using the Optimized Hot Spot analysis tool in ArcGIS, which aggregated data using a 40km fishnet and the Getis-Ord Gi* statistic. Seasonal analysis revealed several differences in hot spot location dependent upon ENSO phase. Winter showed a northward expansion in tornado hot spots as ENSO transitioned from Moderate El Niño to Moderate La Niña, which was further verified with difference maps and atmospheric composites. Spring exhibited an eastward expansion in tornado hot spots from Moderate El Niño to Weak La Niña in the central U.S., and summer showed a similar geographical distribution in the northern United States regardless of ENSO phase. Fall

did not exhibit a uniform pattern dependent upon ENSO phase, however hot spots were more aggregated during El Niño phases and dispersed during La Niña phases. This was verified with global statistics. Weak and strong tornado hot spot analysis revealed several interesting differences in location during Strong El Niño in fall and winter, as well as Spring Weak La Niña, but a majority of hot spot locations between EF01 and EF25 tornadoes were not anomalous from the all tornado record hot spot analysis. These results confirm the hypothesis that ENSO has an influence on tornado activity in the eastern United States predominately during winter and spring.

4.3 Objective 3 – Tornado days and track area as a function of ENSO

To better understand the influence ENSO may have on tornado outbreaks and track area, tornado days (a day with 6 or more tornadoes) were analyzed to compute a Destruction Potential Index (DPI). The resulting DPI values were averaged and analyzed across ENSO intensity and phase to determine whether ENSO plays a role in stronger, longer-lived tornadoes as well as tornado outbreaks. Results for tornado days and DPI were tested for significance using the chi-squared statistic. For summer and fall, the null hypothesis that the frequency of tornado days over the eastern U.S. is independent of ENSO phase could not be rejected. However, winter and spring showed significant chi-square results meaning we can reject the null hypothesis and that ENSO does not have an influence on tornado days during these seasons. When comparing the average DPI across ENSO seasons, a significant chi-square was computed for all four seasons indicating that average DPI is not independent of ENSO phase. Seasonally, winter has the highest DPI during Moderate La Niña. Spring has its largest DPI average during Weak La Niña, and fall has its largest average DPI during Moderate El Niño. Summer resulted in significantly small average DPI values across all phases of ENSO, though it had the second highest number of

outbreaks across the four seasons. This indicates that even though summer is conducive for tornado outbreaks, the tornadoes in these outbreaks are weak and short-tracked. These results meet the third objective, and show us that ENSO does have an influence on tornado days and track area in the eastern U.S.

4.4 Objective 4 – Conflicting results in the literature

The driving force behind this analysis was conflicting results in the literature on the tornado-ENSO relationship. While a majority of studies found that La Niña is favorable for larger annual frequencies, and strong, long-tracked tornadoes, several studies found opposite conflicting results. This analysis revealed geographic patterns and annual frequencies which confirmed that La Niña phases generally have a larger influence on tornadic activity in the eastern United States. Possibly more important, this study revealed that the intensity of ENSO does play a role in tornadic frequency and geographic distribution seasonally, and should not be neglected. This study also showed an improvement in the current literature by examining the role of ENSO during all four seasons, and not just tornado peak seasons. Therefore, with confidence we can say that this analysis greatly met the final objective of this study – to clarify varying results in the tornado-ENSO relationship.

4.5 Limitations

One of the largest limitations in this study was the tornado database. The increase in tornado reports due to technology advancement, urbanization, increased eyewitness reports, and increased structures for damage reports have led to a large spike in the overall observational record. While this can be remedied with the SPC linear regression method, it is still a fallback for analyses conducted as far back as 1950. Lastly, there is a limitation with these types of studies due to a scaling problem. Tornadoes are considered mesoscale, whereas ENSO is large-scale and

long-term atmospheric process, making it difficult to attribute tornadic frequencies and spatial distribution without careful analysis.

4.6 Future Work

There is work that can still be done with the tornado-ENSO relationship utilizing a seven-classification system instead of the traditional three-classification system. Potential future work could determine a way to statistically test the geographic differences between tornado hot spots by ENSO phase, instead of qualitatively analyzing the differences. As discussed in Chapter 3, a mesoscale analysis on weak versus strong tornadoes is necessary to understand ENSO-related influences on tornado intensity in the eastern U.S. Other potential expansions of this analysis could include potential for injuries, deaths, and tornado duration dependent upon ENSO intensity and phase. Improvement in these types of study could result from a longer study period, increasing the sample sizes in the stronger ENSO categories revealing a more detailed hot spot analysis for Strong and Moderate El Niño/La Niña. Perhaps most importantly, future research could also utilize the seasonal findings of this study through machine-based learning to create a functional prediction tool, which has been studied previously but only for spring (LaCorte 2011).

REFERENCES

Aerd. "Kruskal-Wallis H Test Using SPSS Statistics." *Kruskal-Wallis H Test in SPSS Statistics | Procedure, Output and Interpretation of the Output Using a Relevant Example.* Aerd Statistics, 2016. Web. 19 Jan. 2017.

Allen, J. T., et al. (2015). "Influence of the El Niño/Southern Oscillation on tornado and hail frequency in the United States." Nature Geoscience 8(4): 278-283.

AMS. "Precipitable Water." *Precipitable Water - AMS Glossary*. American Meteorological Society, 13 Jan. 2015. Web. 27 Mar. 2017. <http://glossary.ametsoc.org/wiki/Precipitable_water>.

Archer, C. L. and K. Caldeira (2008). "Historical trends in the jet streams." Geophysical Research Letters 35(8): n/a-n/a.

Barnes, S. and C. Newton (1986). "Thunderstorms in the synoptic setting." Thunderstorm morphology and dynamics 1: 2.

Brooks, Harold, and Greg Carbin. "Inflation Adjusted Tornado Running Totals - Storm Prediction Center WCM Page." *Inflation Adjusted Tornado Running Totals - Storm Prediction Center WCM Page*. Storm Prediction Center, 2007. Web. 19 Jan. 2017.

Center, S. P. (2016). "Storm Prediction Center WCM Page." from http://www.spc.noaa.gov/wcm/#data.

Cook, A. R. and J. T. Schaefer (2008). "The relation of El Niño-Southern Oscillation (ENSO) to winter tornado outbreaks." Monthly Weather Review 136(8): 3121-3137.

CPC. "Climate Prediction Center - Monitoring & Data: Current Monthly Atmospheric and Sea Surface Temperatures Index Values." *Climate Prediction Center - Monitoring & Data: Current Monthly Atmospheric and Sea Surface Temperatures Index Values*. NOAA Center for Weather and Climate Prediction, 2016. Web. 19 Jan. 2017.

"Downloads | Natural Earth." *Natural Earth Downloads*. Natural Earth, 2016. Web. 19 Jan. 2017.

Drakoen , 8:51 PM GMT on June 17, 2008, Drakoen. "Geopotential Heights." *Geopotential Heights | Drakoen's WunderBlog*. Wunderground, 17 June 2008. Web. 19 Jan. 2017.

Eichler, T. and W. Higgins (2006). "Climatology and ENSO-related variability of North American extratropical cyclone activity." Journal of Climate 19(10): 2076-2093.

ESRI. "ArcGIS Pro." *Spatial Autocorrelation (Global Moran's I)—ArcGIS Pro | ArcGIS Desktop*. ArcMap, 2016. Web. 19 Jan. 2017.

ESRI. "Average Nearest Neighbor (Spatial Statistics)." *Average Nearest Neighbor (Spatial Statistics)*. ArcMap, 2016. Web. 19 Jan. 2017.

ESRI. "Help." *Lambert Conformal Conic—Help | ArcGIS for Desktop*. ArcMap, 2016. Web. 19 Jan. 2017.

ESRI. "Help." *Optimized Hot Spot Analysis—Help | ArcGIS for Desktop*. ArcMap, 2016. Web. 19 Jan. 2017.

ESRL. "Physical Sciences Division." *ESRL Monthly/Seasonal Climate Composites*. NOAA Center for Weather and Climate Prediction, 2016. Web. 19 Jan. 2017. https://www.esrl.noaa.gov/psd/cgi-bin/data/composites/printpage.pl

Farney, T. J. and P. G. Dixon (2015). "Variability of tornado climatology across the continental United States." International Journal of Climatology 35(10): 2993-3006.

Farney, T. J. and P. G. Dixon (2015). "Variability of tornado climatology across the continental United States." International Journal of Climatology 35(10): 2993-3006.

Frauenfeld, O. W. and R. E. Davis (2003). "Northern Hemisphere circumpolar vortex trends and climate change implications." Journal of Geophysical Research: Atmospheres 108(D14): n/a-n/a.

Haby, Jeff. "Severe Thunderstorm Ingredients." *Wind Shear*. The Weather Prediction, 2016. Web. 30 Nov. 2016.

Hardy, J. W. and S. Hsu (1997). "A climatology of winter cyclogenesis intensity in the northwest Gulf of Mexico." Natl Weather Dig 22: 3-7.

Holton, J. R. (1992). "An introduction to dynamic meteorology Academic Press." San Diego.

Johns, Robert H., and Charles A. Doswell III. "Severe local storms forecasting." *Weather and Forecasting* 7.4 (1992): 588-612.

"Kruskal-Wallis and Friedman Tests." *Kruskal-Wallis and Friedman Tests*. Bournemouth University, 2016. Web. 19 Jan. 2017.

LaCorte, Sandra. "A Neural Network Approach to Tornado Forecasting in North Alabama and Southern Middle Tennessee." Thesis. The University of Alabama in Huntsville, 2011. Web. 1 Apr. 2017. <http://www.nsstc.uah.edu/sundar/papers/2011/LaCorte_thesis_final.pdf>.

Lee, S. K., et al. (2013). "Is There an Optimal ENSO Pattern That Enhances Large-Scale Atmospheric Processes Conducive to Tornado Outbreaks in the United States?" Journal of Climate 26(5): 1626-1642.

Lee, S.-K., et al. (2016). "US regional tornado outbreaks and their links to spring ENSO phases and North Atlantic SST variability." Environmental Research Letters 11(4): 044008.

Marzban, C. and J. T. Schaefer (2001). "The Correlation between U.S. Tornadoes and Pacific Sea Surface Temperatures." Monthly Weather Review 129(4): 884-895.

McKight, P. E. and Najab, J. 2010. Kruskal-Wallis Test. Corsini Encyclopedia of Psychology. 1..

Mercer, A. E., et al. (2012). "Synoptic composites of tornadic and nontornadic outbreaks." Monthly Weather Review 140(8): 2590-2608.

Monfredo, W. (1999). "Relationships between phases of the El Niño-Southern Oscillation and character of the tornado season in the south-central United States." Physical Geography 20(5): 413-421.

NOAA. "Glossary." *Glossary*. NOAA's National Weather Service, 2017. Web. 23 Feb. 2017.

NCSU. "Geopotential Height." *Geopotential Height*. State Climate Office of North Carolina, 2016. Web. 19 Jan. 2017.

NSSL. "Thunderstorm Basics." *NOAA National Severe Storms Laboratory*. NOAA's NSSL, 2016. Web. 30 Nov. 2016.

Null, J. (2016, February 4, 2016). "El Niño and La Niña Years and Intensities." from http://ggweather.com/enso/oni.htm.

NWS. "Glossary." *Lifted Index*. NOAA, 25 June 2009. Web. 27 Mar. 2017. <http://w1.weather.gov/glossary/index.php?word=lifted%2Bindex>.

Patrick Royston (1982) Algorithm AS 181: The *W* test for Normality. *Applied Statistics*, **31**, 176–180.

R Core Team. *R*. Computer software. *R: A Language and Environment for Statistical Computing*. Vers. 3.3.2. R Foundation for Statistical Computing, 2016. Web. 17 Jan. 2017.

Schaefer, J., et al. (1980). Tornado track characteristics and hazard probabilities. 5th Int. Conf. on Wind Engrg, July.

Schaefer, J. and R. Edwards (1999). The SPC tornado/severe thunderstorm database. Preprints, 11th Conf. on Applied Climatology, Dallas, TX, Amer. Meteor. Soc.

Schultz, D. M., et al. (2014). "Tornadoes in the Central United States and the “Clash of Air Masses”." Bulletin of the American Meteorological Society 95(11): 1704-1712.

Schultz, D. M., et al. (2014). "Tornadoes in the Central United States and the “Clash of Air Masses”." Bulletin of the American Meteorological Society 95(11): 1704-1712.

SPC. "Severe Weather Climatology - Gridded Areas." *Severe Weather Climatology - Gridded Areas*. NOAA Center for Weather and Climate Prediction, 2016. Web. 19 Jan. 2017.

SPC. (2016). "Storm Prediction Center WCM Page." from http://www.spc.noaa.gov/wcm/#data.

Thompson, R. L. and M. D. Vescio (1998). The destruction potential index—A method for comparing tornado days. Preprints, 19th Conf. on Severe Local Storms, Minneapolis, MN, Amer. Meteor. Soc.

"Troughs: Upper Level Lows." *Troughs: Upper Level Lows*. University of Illinois, 2010. Web. 19 Jan. 2017.

USC. "Spatial Statistics." *USC Health Sciences Campus*. Web. 19 Jan. 2017.

Vries, A. D., & Meys, J. (2015). *R For Dummies, 2nd Edition*. John Wiley & Sons.

Wilks, D. S. (2011). Chapter 5 - Frequentist Statistical Inference. International Geophysics. S. W. Daniel, Academic Press. Volume 100: 133-186.

APPENDIX

Table A.1. Seasonally binned Strong El Niño years from 1950 through 2014.

Winter (DJF)	Spring (MAM)	Summer (JJA)	Fall (SON)
1957-1958			1965
1972-1973			1972
1982-1983			1982
1991-1992			1997
1997-1998			

Table A.2. Seasonally binned Moderate El Niño years from 1950 through 2014.

Winter (DJF)	Spring (MAM)	Summer (JJA)	Fall (SON)
1965-1966	1983	1957	1957
1986-1987	1992	1965	1963
2009-2010		1972	1987
		1987	2002
		1997	

Table A.3. Seasonally binned Weak El Niño years from 1950 through 2014.

Winter (DJF)	Spring (MAM)	Summer (JJA)	Fall (SON)
1952-1953	1953	1953	1951
1953-1954	1957	1963	1953
1958-1959	1958	1982	1958
1963-1964	1966	1991	1969
1968-1969	1969	2002	1976
1969-1970	1987		1977
1976-1977	1993		1986
1977-1978	1998		1991
1979-1980			1994
1987-1988			2004
1994-1955			2006
2002-2003			2009
2004-2005			
2006-2007			
2014-2015			

Table A.4. Seasonally binned Neutral years from 1950 through 2014.

Winter (DJF)	Spring (MAM)	Summer (JJA)	Fall (SON)
1951-1952	1951	1951	1952
1956-1957	1952	1952	1956
1959-1960	1954	1956	1959
1960-1961	1959	1958	1960
1961-1962	1960	1959	1961
1962-1963	1961	1960	1962
1966-1967	1962	1961	1966
1978-1979	1963	1962	1967
1980-1981	1964	1966	1968
1981-1982	1965	1967	1978
1983-1984	1967	1968	1979
1985-1986	1970	1969	1980
1989-1990	1972	1976	1981
1990-1991	1973	1977	1985
1992-1993	1976	1978	1989
1993-1994	1977	1979	1990
2001-2002	1978	1980	1992
2003-2004	1979	1981	1993
2008-2009	1980	1983	1996
2012-2013	1981	1984	2001
2013-2014	1982	1985	2003
	1984	1986	2005
	1986	1989	2008
	1988	1990	2012
	1990	1992	2013
	1991	1993	2014
	1994	1994	
	1995	1995	
	1996	1996	
	1997	2001	
	2001	2003	
	2002	2004	
	2003	2005	
	2004	2006	
	2005	2007	
	2006	2008	
	2007	2009	
	2009	2011	
	2010	2012	
	2012	2013	
	2013	2014	
	2014		

Table A.5. Seasonally binned Weak La Niña years from 1950 through 2014.

Winter (DJF)	Spring (MAM)	Summer (JJA)	Fall (SON)
1950-1951	1955	1950	1950
1954-1955	1956	1954	1954
1955-1956	1968	1955	1964
1964-1965	1971	1964	1970
1967-1968	1974	1970	1971
1971-1972	1975	1971	1974
1974-1975	1985	1973	1983
1984-1985	1989	1974	1984
1995-1996	1999	1998	1995
1996-1997	2000	2000	2000
2000-2001	2008	2010	2011
2005-2006	2011		
2011-2012			

Table A.6. Seasonally binned Moderate La Niña years from 1950 through 2014.

Winter (DJF)	Spring (MAM)	Summer (JJA)	Fall (SON)
1970-1971	1950	1975	1955
1975-1976		1988	1975
1998-1999		1999	1988
2007-2008			1998
2010-2011			1999
			2007
			2010

Table A.7. Seasonally binned Strong La Niña years from 1950 through 2014.

Winter (DJF)	Spring (MAM)	Summer (JJA)	Fall (SON)
1973-1974			1973
1988-1989			
1999-2000			

VITA

Coryn Collins, a native to Coppell, Texas, received her bachelor's degree in meteorology with a minor in mathematics from Texas A&M University in May 2015. The following fall semester, she moved to Baton Rouge, LA, to enroll in the Department of Geography and Anthropology at Louisiana State University to pursue a master's in geography, specializing in climatology. She expects to receive her master's degree in May 2017, and plans on moving to Texas upon graduation to find a job closer to home.